



*Industry Compliant Wireless Power and Data Transfer Module Towards Ensuring Battery Denial of Service Protection*

**Vasileios Skrekas**

# Industry Compliant Wireless Power and Data Transfer Module Towards Ensuring Battery Denial of Service Protection

By

Vasileios Skrekas

in partial fulfilment of the requirements for the degree of

**Master of Science**

Biomedical Engineering

at Delft University of Technology,

to be defended publicly on Wednesday April 29, 2020 at 10:00 AM.

|                   |  |                                    |
|-------------------|--|------------------------------------|
| Supervisors:      | Prof. dr. ir. W.A. Serdijn,<br>Dr. C. Strydis, | TU Delft<br>Erasmus Medical Centre |
| Thesis committee: | Dr. V. Valente,<br>Dr. S. Izadkhast,           | TU Delft<br>TU Delft               |



# Abstract

The field of active implantable medical devices (IMDs) has made huge steps forward in the last years. IMDs are used today for the treatment of previously untreatable conditions as well as the continuous monitoring of the health of patients. The field, where active IMDs have been the most successful, is the field of neurological conditions, on which traditional medicine such as the intake of pills has very limited effect. In order to take full advantage of the possibilities offered by the IMDs it is vital to have communication between them and the external world. In this way, the treatment method provided by the IMD can be configured and optimized for each separate individual, achieving the best possible results. Moreover, the state of the device itself can be assessed and therefore possible flaws in its operation can be detected and corrected. Finally, in case of monitoring the patient's health condition communication is also vital.

However, this communication between the external world and the implanted device also introduces the possibility for someone, that possesses the required expertise and skills, to hack the device. The hacker can possibly "eavesdrop" the communication channel in order to extract information regarding the patient or even act in order to change parameters of the device and the therapy it provides, possibly causing harm to the patient. One way for hackers to disrupt the normal operation of the IMD is to drain its power source, namely the battery of the device, an attack that is named battery denial of service (BDoS) attack. One of the easiest ways to achieve such an attack is to make the device commit valuable power resources in order to run the authentication protocols continuously, by non-stop requesting for access.

In this thesis, we try to tackle this problem by creating an analog circuit module that can act as an add-on to commercial IMDs that will have the task of authenticating the user that is trying to communicate with the IMD by making use of harvested wireless energy that is required for the communication. In this way, we expect to relieve the IMDs from spending time and resources on the authentication process. To that end, we designed and created an analog experimental prototype that employs both wireless power transfer and data communication, by simply making use of off-the-shelf components. The goal of this experimental prototype is to identify further challenges that can arise in a so called zero power defence scenario.

To that end we implement a system that makes use of near-field resonant inductive coupling as a wireless power transfer method and is able to provide some mW of power across distances of up to 2cm, an amount of power that is sufficient to drive a microcontroller that can execute a low power security protocol in order to authenticate the entity trying to access the receiver. In addition to that, it can achieve a downlink data rate of 200kbit/s using amplitude shift keying modulation and an uplink data rate of 1kbit/s by making use of passive load shift keying modulation.

This system is a unique implementation, since it constitutes the only solution that implements a highly asymmetrical bidirectional link by making use of ASK and LSK modulation and has a completely wirelessly powered receiver. Moreover, since this implementation was achieved with simple off-the-shelf components, there is a large margin of improvement in terms of size and efficiency if such a system was to be designed as an ASIC.



# Acknowledgements

I would like to express my deep gratitude to all the people who have contributed in any possible way to my academic journey in TU Delft these last two and a half years and helped me evolve as an engineer and as a person in general.

First of all, I would like to thank Professor Wouter A. Serdijn, and head of the Bioelectronics group of TU Delft, for his guidance and support during the hard process of this project. You were always there when I had questions and when I needed your counsel. Even when I was facing difficulties you always gave the nudge I needed to move forward both project-wise and mentally. You are an amazing professor and mentor and I could not have asked for a better supervisor.

I would also like to thank Assistant Professor Christos Strydis and PhD candidate M. Ali Siddiqi from the Neuroscience department of Erasmus Medical Centre, Rotterdam, for entrusting me with their idea about zero power defence that gave life to this thesis project. I also thank them for the cooperation and support they offered me and from allowing me to see the design of an IMD from a completely different perspective.

Many thanks also to the people of Bioelectronics group that always create a very warm and lively atmosphere at the thirteenth floor of EWI and are always willing to help and provide their insight. Special thanks to Vivo, whose advice has been vital in the design of the experimental prototype of this thesis.

My deepest thanks goes also to my friends and my girlfriend, who have helped me fill these years with wonderful and precious memories that I will cherish for the rest of my life. You supported me all the way from the beginning and I could never have done this without you all.

Finally, I would like to express my deepest gratitude to my family. You never stopped believing in me and you provided me with the all the resources I needed to achieve what I have achieved in my life. You made me who I am today and I will never stop trying to make you proud. I love you from the bottom of my heart.

# Table of Contents

|   |           |
|---|-----------|
| Abstract.....   | iv        |
| Acknowledgements.....   | vi        |
| Table of Contents.....  | vii       |
| List of Abbreviations.....  | ix        |
| List of Figures.....  | x         |
| List of Tables.....   | xii       |
| <b>1 Introduction.....</b>  | <b>1</b>  |
| 1.1 The Need for Wireless Connectivity and the Arising Risks..... | 1         |
| <b>2 Literature Study.....</b>                                    | <b>4</b>  |
| 2.1 Safety Boundaries.....  | 4         |
| 2.2 Wireless Power Transfer.....                                  | 5         |
| 2.2.1 Electromagnetic Radiation Regions.....                      | 5         |
| 2.2.2 Ultrasound Field Regions.....                               | 6         |
| 2.2.3 Near-field Resonant Inductive Coupling.....                 | 6         |
| 2.2.4 Near-field Capacitive Coupling.....                         | 9         |
| 2.2.5 Ultrasonic Energy Transfer.....                             | 10        |
| 2.2.6 Far Field Wireless Power Transfer.....                      | 11        |
| 2.2.7 Comparison of Wireless Power Transfer Methods.....          | 12        |
| 2.3 Data Modulation.....  | 13        |
| 2.3.1 Amplitude Shift Keying.....                                 | 14        |
| 2.3.2 Frequency Shift Keying.....                                 | 16        |
| 2.3.3 Phase Shift Keying.....                                     | 18        |
| 2.3.4 Comparison of Data Modulation Techniques.....               | 19        |
| 2.3.5 Research Questions.....                                     | 20        |
| <b>3 System Overview.....</b>                                     | <b>21</b> |
| 3.1 System Description.....                                       | 21        |
| 3.2 System Characteristics.....                                   | 22        |
| <b>4 Circuit Design.....</b>                                      | <b>23</b> |
| 4.1 Transmitter.....  | 23        |
| 4.1.1 Antenna.....  | 23        |
| 4.1.2 Class-E Amplifier.....                                      | 23        |

|   |           |
|---|-----------|
| 4.1.3 ASK Modulator.....                                    | 26        |
| 4.1.4 ASK Demodulator.....                                  | 27        |
| 4.2 Receiver.....   | 29        |
| 4.2.1 Antenna.....  | 29        |
| 4.2.2 Rectifier and Storage Unit.....                       | 29        |
| 4.2.3 ASK Demodulator.....                                  | 31        |
| 4.2.4 Backscattering.....                                   | 31        |
| <b>5 Prototype Design.....</b>                              | <b>33</b> |
| 5.1 Introduction.....                                       | 33        |
| 5.2 Component Selection.....                                | 33        |
| 5.3 PCB Design and Assembly.....                            | 36        |
| <b>6 Measurements and Characterization of the Link.....</b> | <b>38</b> |
| 6.1 Measurement Setup and Additional Equipment.....         | 38        |
| 6.2 Limitations.....  | 39        |
| 6.3 Measurements.....                                       | 39        |
| 6.3.1 Receiver Detuning.....                                | 39        |
| 6.3.2 Wireless Power Transfer.....                          | 39        |
| 6.3.2 Maximum Detectable Frequency.....                     | 42        |
| 6.4 Backscattering.....                                     | 44        |
| 6.5 Result Summary.....                                     | 45        |
| <b>7 Conclusions.....</b>                                   | <b>47</b> |
| 7.1 Contributions.....                                      | 47        |
| 7.2 Discussion.....   | 47        |
| 7.3 Recommendations for future work.....                    | 48        |
| Bibliography.....   | 49        |

# List of Abbreviations

|       |   |
|-------|---|
| IMD   | Implantable Medical Device              |
| BDoS  | Battery Denial of Service               |
| MITM  | Man In The Middle                       |
| ZPD   | Zero Power Defence                      |
| EM    | Electromagnetic                         |
| WPT   | Wireless Power Transfer                 |
| BRs   | Basic Restrictions                      |
| SAR   | Specific Absorption Rate                |
| RF    | Radio Frequency                         |
| NRIC  | Near Field Resonant Inductive Coupling  |
| PTE   | Power Transfer Efficiency               |
| EMF   | Electromotive Force                     |
| PA    | Power Amplifier                         |
| OOK   | On/Off Keying                           |
| ASK   | Amplitude Shift Keying                  |
| FSK   | Frequency Shift Keying                  |
| PSK   | Phase Shift Keying                      |
| NFCC  | Near Field Capacitive Coupling          |
| UET   | Ultrasonic Energy Transfer              |
| PZT   | Lead-Zirconate Titanate                 |
| WBAN  | Wireless Body Area Network              |
| QAM   | Quadrature Amplitude Modulation         |
| QPSK  | Quadrature phase shift keying           |
| DPSK  | Differential Phase Shift Keying         |
| LSK   | Load Shift Keying                       |
| VCO   | Voltage Controlled Oscillator           |
| LPF   | Low Pass Filter                         |
| ISM   | Industrial, Scientific, Medical         |
| BPSK  | Binary Phase Shift Keying               |
| OQPSK | Offset Quadrature Phase Shift Keying    |
| ASIC  | Application Specific Integrated Circuit |
| PCB   | Printed Circuit Board                   |
| IC    | Integrated Circuit                      |

# List of Figures

|  |    |
|--|----|
| Figure 1 . Man-in-the-middle attacks.....  | 2  |
| Figure 2 . Battery denial of service attacks.....  | 2  |
| Figure 3 . Block diagram of a WPT system for IMDs.....   | 5  |
| Figure 4 . E/M radiation regions.....  | 5  |
| Figure 5 . Ultrasound field pattern geometry [12].....   | 6  |
| Figure 6 . Near-field inductive power transfer [1].....  | 7  |
| Figure 7 . System level block diagram of NRIC WPT method [13].....   | 8  |
| Figure 8 . Near-field capacitive coupling WPT [22].....  | 9  |
| Figure 9 . Schematic of UET method [1].....  | 10 |
| Figure 10 . State of the art UET system [25].....  | 11 |
| Figure 11 . Far-field WPT Scheme [27].....   | 12 |
| Figure 12 . Energy profile of a sensor with duty cycle operation and a far-field WPT scheme [3].....   | 12 |
| Figure 13 . Power transfer capability, data rates and complexity of the transmission barrier comparison  | 13 |
| Figure 14 . Binary digital modulation schemes: (a) ASK, (b) PSK and (c) FSK [9].....   | 14 |
| Figure 15 . M-ary modulation. (A) M-ASK, (B) M-FSK, (C) M-PSK [32].....  | 14 |
| Figure 16 . OOK modulation .....   | 15 |
| Figure 17 . Asynchronous ASK demodulator.....  | 16 |
| Figure 18 . Binary FSK modulator.....  | 17 |
| Figure 19 . Asynchronous FSK demodulator .....   | 17 |
| Figure 20 . Synchronous FSK demodulator .....  | 17 |
| Figure 21 . Binary PSK modulator.....  | 18 |
| Figure 22 . COSTAS loop BPSK demodulator [29].....   | 19 |
| Figure 23 . Proposed system-level block diagram.....   | 21 |
| Figure 24 . Class-E amplifier typical topology [51].....   | 23 |
| Figure 25 . Ideal waveforms of class-E amplifier operation for maximum power efficiency. (a) Voltage across the switch. (b) Current through the switch [48]..... | 24 |
| Figure 26 . Class E amplifier and transmitting antenna.....  | 25 |
| Figure 27 . Data modulation and power transfer [50].....   | 26 |
| Figure 28 . ASK modulator, power amplifier and transmitting coil.....  | 27 |
| Figure 29 . ASK demodulation scheme.....   | 28 |
| Figure 30 . Uplink data demodulator.....   | 28 |

|   |           |
|---|-----------|
| <i>Figure 31 . General charge pump rectifier topology [52].....</i>   | <i>30</i> |
| <i>Figure 32 . Receiving coil, charge pump rectifier and load schematic.....</i>  | <i>30</i> |
| <i>Figure 33 . ASK demodulator at the receiving side.....</i>   | <i>31</i> |
| <i>Figure 34 . Receiver with backscattering.....</i>  | <i>32</i> |
| <i>Figure 35 . PCB design of the transmitter.....</i>   | <i>36</i> |
| <i>Figure 36 . PCB design of the receiver.....</i>  | <i>36</i> |
| <i>Figure 37 . Transmitter PCB.....</i>   | <i>37</i> |
| <i>Figure 38 . Receiver PCB.....</i>  | <i>37</i> |
| <i>Figure 39 . Complete measurement setup.....</i>  | <i>38</i> |
| <i>Figure 40 . Output voltage and demodulated signal.....</i>   | <i>39</i> |
| <i>Figure 41 . Output power over distance with 3V supply.....</i>   | <i>40</i> |
| <i>Figure 42 . Output power over distance with 4V supply.....</i>   | <i>41</i> |
| <i>Figure 43 . Output power over distance with 5V supply.....</i>   | <i>41</i> |
| <i>Figure 44 . Output power over Distance with 6V supply.....</i>   | <i>42</i> |
| <i>Figure 45 . Received downlink modulated signal (pink) and demodulated signal (teal).....</i>   | <i>42</i> |
| <i>Figure 46 . Maximum detectable modulation frequencies over distance.....</i>   | <i>43</i> |
| <i>Figure 47 . Transmitted signal (teal) and demodulated data (yellow) with MI = 22.9%.....</i>   | <i>43</i> |
| <i>Figure 48 . Transmitted signal (teal) and demodulated data (yellow) with MI = 36.6%.....</i>   | <i>44</i> |
| <i>Figure 49 . Transmitted signal (teal) during backscattering and demodulated uplink signal (yellow).....</i>  | <i>44</i> |
| <i>Figure 50 . Simulation waveforms of backscattered a) envelope detected signal (blue), b) averaged (green) and c) demodulated signal (red).....</i> | <i>45</i> |

# List of Tables

|   |    |
|---|----|
| <i>Table 1 BRs for frequencies between 100kHz and 3 GHz</i> .....         | 4  |
| <i>Table 2 . Inductive Power Transfer Summary</i> .....                   | 9  |
| <i>Table 3 . Near Field Capacitive Coupling Power Transfer [22]</i> ..... | 10 |
| <i>Table 4 . Selected Transistors</i> .....                               | 33 |
| <i>Table 5 . Selected Capacitors</i> .....                                | 34 |
| <i>Table 6 . Selected Diodes</i> .....                                    | 34 |
| <i>Table 7 . Selected Resistors</i> .....                                 | 35 |
| <i>Table 8 . Selected Inductors</i> .....                                 | 35 |
| <i>Table 9 . Selected Comparator</i> .....                                | 35 |
| <i>Table 10 . Additional Lab Equipment</i> .....                          | 38 |
| <i>Table 11 . Comparison Table</i> .....                                  | 47 |

# 1 Introduction

## 1.1 The Need for Wireless Connectivity and the Arising Risks

Active implantable medical devices (IMDs) are on the rise across the last decades. This can easily be understood by simply emphasizing the fact that an increasing number of university as well as company groups around the world are involved in conducting research on diagnostic, therapeutic as well as monitoring IMDs. This has been facilitated by the better understanding of the physiology of the human body, the use of better and more biocompatible materials, the development and/or improving of sensors that allow us to take measurements inside the human body safely and accurately while using minimal power, the refining of packaging technologies as well as the ever decreasing size of electronics and integrated circuits, which has allowed the power efficiency and therefore the lifetime of implantable devices to be dramatically augmented, [1], [2], [3].

This, however, also increases the complexity of these devices and makes the wireless communication and data exchange between them and an outside source necessary, so that configuration and optimization of the therapy can be provided in order to get the best possible results, diagnostics regarding the integrity of the device itself can be run and updates can take place effectively and the patient's health condition can be monitored [4], [5]. However, this need for communication between the implanted device and the external reader gives rise to concerns regarding the security of this communication and its vulnerability to attacks, namely hacking incidents. A possible attacker may exploit the functionality of the IMD in order to steal information or even cause harm to the patient. These attacks can be categorized as:

- **Passive:** The attacker eavesdrops the communication channel between the IMD and the reader and can extract information on the therapy as well as the patients themselves.
- **Active:** The attacker is able to launch commands for execution at the IMD, that may change its regular function or even execute commands that cause life threatening actions. For example, one could exploit the function of a defibrillator in order to deliver a strong shock to a patient, or even induce arrhythmia.

Recently, a number of security vulnerabilities of IMDs have been identified, which are mainly related to the transmission of unencrypted data, the use of very weak authentication techniques, the inefficient protection from battery depletion attacks, and the absence of efficient accounting techniques to trace sensitive actions to individuals responsible of their executions [6], [7]. Hence, it can be easily understood that security constitutes a major concern; one could say it is the Achilles' Heel of today's implantable devices.

The aforementioned two types of attacks can be achieved through the following ways: the Man-In-The-Middle (MITM) as well as the Battery Denial of Service attacks (BDoS). In the former type of attack, an malicious adversary can eavesdrop the communication channel, replay stored or provide altered pieces of communication between the IMD and the reader without either of the two noticing it [5]. This is depicted in Figure 1.

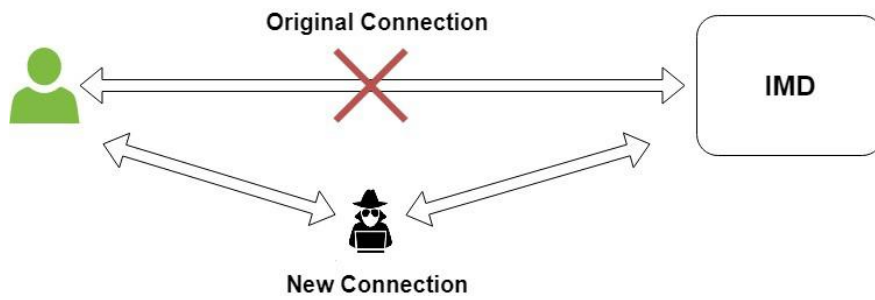


Figure 1. Man-in-the-middle attacks

The MITM attacks pose a threat because they are able to:

- Intercept information regarding the patient's condition and treatment as well as his personal information. This information can be used in order to blackmail the patient or it can be sold to third parties.
- Exploit the simple architecture of some IMDs and store repeated command packets. This allows the attacker to replay the commands, while the IMD will "think" they were provided by a legitimate reader
- Intercept the information sent by the reader, alter it and resend it to the receiver. In this way the IMD executes the commands of the hacker and not the ones that were sent from the physician through the reader

As far as the BDoS attacks are concerned, the attacker forces the device to execute energy-consuming operations in order to deplete the power supply of the IMD, namely the battery and force the shutdown of the device. One way to achieve this would be to constantly send communication requests to the IMD. Hence, the IMD would be forced to ceaselessly execute its security authentication protocols in order to examine and then reject these communication requests, which would undoubtedly deplete the power resources of the device [4]. Such BDoS attacks are depicted in Figure 2.



Figure 2. Battery denial of service attacks

So far, a zero-power notification (in the form of an audible or tactile alert) and zero-power authentication (implementation of a cryptographically strong authentication protocol using harvested energy) have been proposed [6]. It has also been proposed to make use of the patient's physiological parameters in the authentication process by using an easily measurable parameter from both the outside as well as from the inside of the body as an authentication key [7], [8].

The Neuroscience department of Erasmus Medical Centre in Rotterdam has been working for some time on the security aspect of IMDs and specifically on the alleviation of the Battery Denial of service attacks, that constitute a global threat for any IMD that makes use of wireless communication. This was the stimulus that started the idea behind this thesis, where we try to tackle the BDoS attacks, by designing an analog circuit module meant to act as an add-on to the IMDs that will harvest energy from the entity that is trying to establish communication with the IMD in order to execute the authentication process and save the time as well as the resources from the side of the IMD, thus incorporating the Zero Power Defence (ZPD) scheme. In order to do so, a power efficient authentication protocol created by the author of [8] will be used.

The thesis is organized in the following manner: First of all, in Chapter 2, we included the literature survey that was conducted in the domains of wireless power transfer and data modulation. The information presented in Chapter 2 is going to be combined with the system description and requirements, presented in Chapter 3 in order to choose the combination of the previously presented wireless power and data transfer methods that suits the proposed application the most. Moreover, the reasoning behind the implementation of the proof-of-concept experimental prototype is presented in this Chapter. This will lead to the selection of the suitable building blocks (sub-circuits) that will constitute our prototype. The design of these building blocks is presented in detail in Chapter 4. Chapter 5 includes the details regarding the selection of the components of these sub-circuits as well as the design of printed circuit boards. The experimental setup along with the acquired measurements constitute Chapter 6. In the final Chapter of this thesis, Chapter 7, conclusions are drawn regarding the viability of the proposed application. Moreover, the measurement results are compared to results presented in published works and propositions for future improvements are made.

# 2 Literature Study

## 2.1 Safety Boundaries

Since we are aiming for a design that will incorporate power as well as data transfer, it makes sense that we focus on these two aspects. However, both these schemes in the majority of their contemporary applications involve the use of electromagnetic (EM) fields, which lead to dissipation of power in the living tissues of the human body. This dissipation can manifest itself as heat, which can cause tissue damage, potentially irreversible. Therefore, when designing a wireless power transfer (WPT) or data telemetry system it is necessary for the designer to make sure that the RF energy generated by the device adheres to the safety levels determined by the standards for the exposure of the human body to RF energy.

For the frequency range of 3 kHz to 300 GHz, where most WPT and telemetry applications are found, the standard used in order to set Basic Restrictions (BRs) on the exposure to Radio Frequency (RF) radiation is the IEEE Std C95.1-2005. These Basic Restrictions are expressed in terms of Specific Absorption Rate (SAR). SAR constitutes a measure of the rate at which energy is absorbed by the human body when exposed to a form of energy. It can be defined as the power absorbed per mass of tissue (W/kg). The relation between SAR and the electric field in every part of the human body is given by the formula:

$$SAR(x, y, z) = \frac{\sigma(x, y, z)E^2(x, y, z)}{2\rho(x, y, z)} \quad (1)$$

where  $\sigma$  is the tissue conductivity (S/m),  $\rho$  is the tissue density (Kg/m<sup>3</sup>) and E stands for the electric field strength (V/m) at a particular point (x,y,z). The SI unit of SAR is watt per kilogram (W/kg). The SAR value depends heavily on the morphology of the part of the body that is exposed to the RF energy as well as on the exact location and geometry of the RF source [9]. Thus, tests must be conducted with each specific source at the specific site of implantation. Table 1 presents the BRs for the whole body and localized exposure not only for people in controlled environments but also for the general public when an RF safety program is unavailable. The localized exposure BRs are expressed in terms of peak spatial-average SAR, which constitutes the maximum local SAR averaged over any 10 grams of body tissue in the shape of a cube [14].

Table 1 BRs for frequencies between 100KHz and 3 GHz

|                            |                                   | SAR(W/kg)            |                                    |
|----------------------------|-----------------------------------|----------------------|------------------------------------|
|                            |                                   | General Public       | Persons in controlled environments |
| <b>Whole-Body Exposure</b> |                                   | Whole Body Average   |                                    |
|                            |                                   | 0.08                 | 0.4                                |
| <b>Localized exposure</b>  | <b>Localized*</b>                 | 2                    | 10                                 |
|                            | <b>Extremities &amp; pinnae**</b> | Peak Spatial Average |                                    |
|                            |                                   | 4                    | 20                                 |

\*Localized in any part of the main body except for the extremities  
 \*\*The extremities are the arms and legs distal from the elbows and knees, respectively, while pinnae are the ear lobes.

In order to come up with an estimation of the electric field as well as the SAR, numerical methods are used. One of the most commonly used numerical techniques in order to estimate electromagnetic-field dosimetry

is the finite-difference time-domain method (FDTD), which constitutes a direct solution of Maxwell's equations in the time domain.

Taking everything into account, every system that incorporates EM transmission and reception should be designed in accordance with the rules regarding the absorption of radiation, whether it has to do with power or data, before it can be considered safe for use on human subjects.

## 2.2 Wireless Power Transfer

The aim of this project is to incorporate both Wireless Power and Data transfer in order to achieve security in the communication with an IMD. First of all, we are going to examine the case of WPT.

A general block diagram of a WPT system is depicted in Figure 3. A transmitter that can be a coil, an antenna, a capacitor or an ultrasonic transducer transmits a signal at a specific frequency. A signal that constitutes a fraction of the initial one is received by the receiver is converted from AC to DC by a rectifier and is finally regulated by a voltage regulator so that it can be used by the implantable device [10].

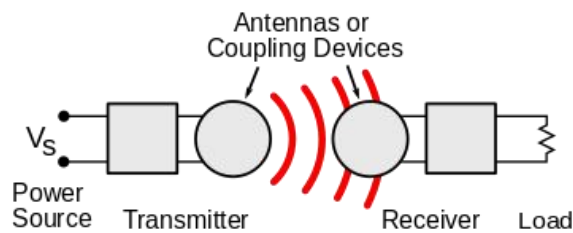


Figure 3. Block diagram of a WPT system for IMDs<sup>i</sup>

Out of the numerous methods that have been proposed during the last few decades, Near-field Inductive, Near-field Capacitive, Ultrasound, Mid-field and Far-field Electromagnetic Coupling methods are either already well-established or show promise in providing power wirelessly to active implantable medical devices [1].

But, before diving deeper in the contemporary methods of WPT it would be beneficial to examine the radiation regions firstly around an antenna and afterwards around an ultrasonic transducer.

### 2.2.1 Electromagnetic Radiation Regions

The space around an antenna can be separated into 2 regions: the near and the far field (Fraunhofer) regions. The near-field region can be further subdivided into two regions: the radiative (Fresnel) and the non-radiative (Reactive) regions. This division is depicted in Figure 4.

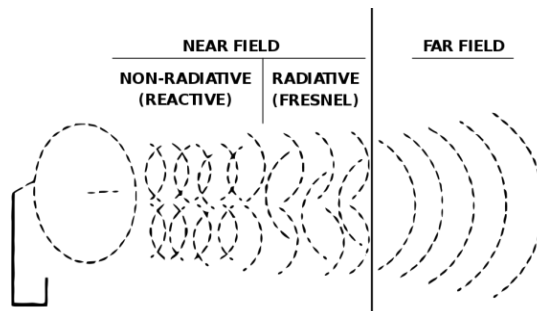


Figure 4. E/M radiation regions<sup>ii</sup>

<sup>i</sup> Retrieved from Wikipedia

<sup>ii</sup> Retrieved from Wikipedia

The reactive near-field region is defined as “the region of the field immediately surrounding the antenna wherein the reactive field predominates.” For the majority of antennas the boundary of this region is usually taken at a distance of  $R < 0.62\sqrt{D^3/\lambda}$  from the antenna, where  $\lambda$  is the wavelength and  $D$  is the largest dimension of the antenna. The Fresnel region is “the region between the reactive and far-field regions wherein radiation fields predominate and the angular field distribution is dependent upon the distance of the antenna.” The distance where this region is found is:  $0.62\sqrt{D^3/\lambda} \leq R \leq 2D^2/\lambda$ . The field pattern is, in general, a function of the radial distance and the radial field component is considerable. The far-field (Fraunhofer) region is defined as “the region of the antenna field where the angular field distribution is essentially independent of the distance from the antenna.” In this region the real part of the Power Density is dominant. This region is found at a distance of  $R \geq 2D^2/\lambda$ . The fields here are transverse to and their angular distribution does not depend on the radial distance [11].

### 2.2.2 Ultrasound Field Regions

The ultrasonic field produced by a transducer is usually geometrically approximated as a cylinder extending from the transducer. This is valid only at extremely short distance from the transducer. Similarly to the electromagnetic radiation, the ultrasonic field further follows the Fresnel and Fraunhofer approximations, where the width of the beam, a.k.a. beamwidth, has different values [12]. This is depicted in Figure 5.

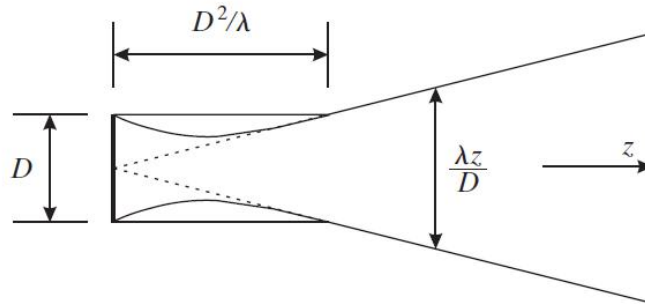


Figure 5. Ultrasound field pattern geometry [12]

We suppose a transducer with diameter  $D$  is pointing at the  $z$ -axis. The geometric region extends from the surface of the transducer until distance  $D^2/4\lambda$  for circular and until  $D^2/2\lambda$  for square transducers. The parameter  $\lambda$  symbolizes the wavelength of the ultrasound beam. The Fresnel region extends from this point up to  $D^2/\lambda$ . After this point is the Fraunhofer, a.k.a far field region, where the ultrasonic beam starts spreading. The beamwidth can be approximated as  $D$  in the geometric and Fresnel regions and  $\lambda z/D$  in the Fraunhofer region. One can observe a “waist” forming in the Fresnel region, which constitutes the point of maximum focus of the beam and therefore the region where the highest lateral resolution is achieved [12].

### 2.2.3 Near-field Resonant Inductive Coupling

The most well-established WPT method regarding IMDs close to the skin surface is the Near-field Resonant Inductive Coupling (NRIC) because of the high Power Transfer Efficiency (PTE) as well as high amounts of power it is able to provide [10]. The mechanism behind power transfer via Inductive Coupling is depicted in Figure 6: an alternating current in the coil at the transmitter’s side creates an alternating magnetic field  $B$  that induces an Electromotive Force (EMF) on the receiving coil by mutual induction, thus creating a voltage. Mutual Induction can be defined as the current flowing in one coil that induces a voltage in an adjacent coil. The mutual inductance of the link is given by the formula:

$$M = \frac{\mu_0 \mu_r N_1 N_2 A}{l} \quad (2)$$

where  $N_1, N_2$  are the number of turns of each coil,  $A$  and  $l$  are the effective area and length of the magnetic path,  $\mu_0$  and  $\mu_r$  are the permeability of free space and the relative permeability of air respectively.

The transmitting coil is found outside the human body, while the receiving coil is implanted in the patient's body at a low depth. From now on the transmitter will be named Tx, the receiver Rx, the transferred power  $P_{TX}$  and the received power  $P_{RX}$ .

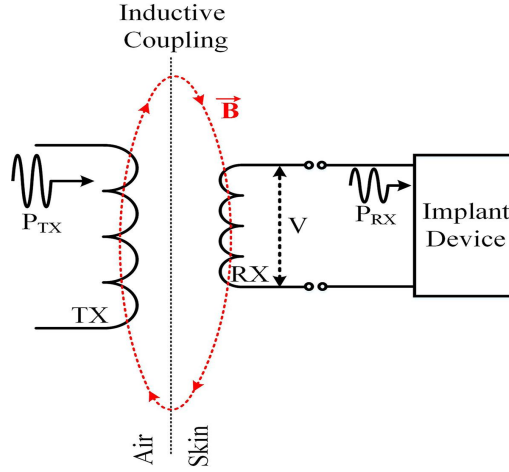


Figure 6. Near-field inductive power transfer [1]

The power-transfer capability of the inductive link needs to be examined further, since it constitutes the cornerstone metric for the evaluation of all the WPT links. Also known as PTE, it can be defined as the ratio of power delivered at the load  $P_{RX}$  to the power drawn from the transmitter  $P_{TX}$ . High link efficiency is always demanded in IMD applications, since it means lower power losses in tissue and the coils.

In order to increase the PTE resonant tuning is used at the receiver side, namely tuning of the receiver at the transmitting frequency. In this way the PTE is maximized under the loose coupling conditions of the link that usually exist in applications where IMDs are involved. The transmitter is in most cases matched to the reflected load in order to decrease the return losses. Maximum PTE is achieved by using a parallel resonant topology at the receiver, which uses large voltage and low current because it constitutes the favorable situation for the rectifiers. Impedance matching can also be used to increase the PTE of the link. In the case where both sides are resonant tuned with the use of two Capacitors  $C_1$  and  $C_2$  the resonant frequency is expressed as:

$$\omega = \frac{1}{\sqrt{L_1 C_1}} = \frac{1}{\sqrt{L_2 C_2}} \quad (3)$$

while the quality factors of the coils are given by:

$$Q_L = \frac{\omega L}{R} \quad (4)$$

where  $L$  is the inductance and  $R$  the internal (series) resistance of each coil. The higher the  $Q$  factor is, the closer an inductor approaches the behaviour of an ideal element. Ideally, we want to have high  $Q$  and low series resistance for the coils used for the link.

In order to simplify the efficiency equations, it is common to normalize the mutual inductance  $M$  of the coils with respect to  $L_1$  and  $L_2$  by defining  $k$ , the coupling coefficient:

$$k = \frac{M}{\sqrt{L_1 L_2}} \quad (5)$$

It can be easily understood that  $k=1$  indicates perfect coupling between the coils while  $k=0$  means that the coils are not coupled at all. Generally speaking, coils with  $k>0.5$  are considered tightly coupled whereas coils with  $k<0.5$  are considered loosely coupled.

The maximum efficiency of the link is given by:

$$\eta_{Max} = \frac{k^2 Q_1 Q_2}{(1 + \sqrt{1 + k^2 Q_1 Q_2})} \quad (6)$$

A system level block diagram of the NRIC WPT method is depicted in Figure 7. The transmitter consists of a power amplifier (PA) that provides a boost to the generated AC signal, before driving the transmitting coil. This generates the alternating magnetic field, which in turn induces the alternating EMF at the receiving end of the link that is then rectified and regulated in order to provide a DC signal to the implant [1], [10], [13].

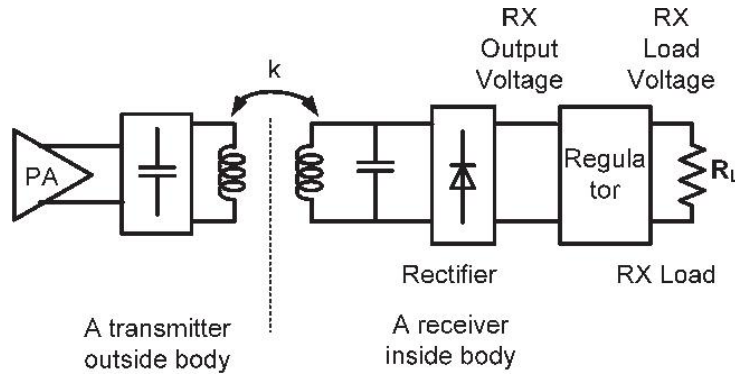


Figure 7. System level block diagram of NRIC WPT method [13]

The overall efficiency of the WPT system depends on the efficiencies of each subsystem in the following manner:

$$\eta_{total} = \eta_{source} \eta_{PTE} \eta_{ac/dc} \quad (7)$$

where  $\eta_{source}$  is the efficiency of the source and the power amplifier,  $\eta_{ac/dc}$  is the rectifier/regulator efficiency and  $\eta_{PTE}$  is the Tx – Rx PTE as was defined earlier. Generally, the source and conversion efficiencies achieve good values. Hence, the whole system efficiency is only limited by the efficiency of the inductive link [1].

The efficiency of the inductive link is heavily dependent on the proper alignment of the coils. The PTE can be severely impaired when the coils are misaligned, as a result of a drop in the mutual inductance as well as the input impedance seen by the PA [14], [15].

Other magnitudes providing design restrictions in a NRIC scheme are the size of the coils, the materials used, the separation length, the frequency used, the geometry of the coils as well as the electrical parameters of the link, namely the inductances of the coils, the mutual inductance, the coupling coefficient etc. [15].

The Inductive link, apart from providing power transfer, is also able to incorporate data telemetry by using techniques such as on/off keying (OOK), amplitude shift keying (ASK), frequency shift keying (FSK) or Phase Shift Keying (PSK) [2], [16]. Data telemetry can be used to communicate with the IMD for the reasons that were stated above. However, data and power telemetry come into contradiction as far as inductive links are concerned, since the former requires a high carrier frequency and a wide frequency band (low Q factor coils) while the latter requires a low carrier frequency and a narrow band (high Q factor coils) [17]. In [18] the authors present an implementation where the power and data links are separated in order to optimize each of them separately at the expense of more space required by the implanted device as well as interference between the links.

Taking everything into account, WPT via Resonant Inductive Coupling is a technique that offers high efficiency, power transfer in the domain of tenths of milliwatts and low rate data transmission at small distances between the coils.

The following table provides a summary of some works on inductive power transfer for IMDs.

Table 2. Inductive power transfer summary

| Work | Power Transferred (mW) | PTE  | Frequency |
|------|------------------------|------|-----------|
| [10] | 102                    | 50%  | 13.56MHz  |
| [14] | 50                     | 36%  | 700kHz    |
| [19] | 11.2                   | 14%  | 13.56MHz  |
| [13] | 174                    | 63%  | 8MHz      |
| [20] | 100                    | 60%  | 13.56MHz  |
| [21] | 1.3                    | 2.4% | 60MHz     |

### 2.2.4 Near-field Capacitive Coupling

Near-field capacitive coupling (NCC) operates under the principle of electric field coupling between two pairs of parallel plates; two of the plates are placed on the implant side while the other two are attached to the skin externally. The skin and the thin layers of tissue act as dielectric [22]. Each pair is used for the forward and reverse current paths. Figure 8 depicts the powering scheme of the capacitive coupling method, which achieves power transfer via the mutual capacitance between the conductors that create a current loop. A constitutes the effective conductor area while D constitutes the length of separation between the plates.

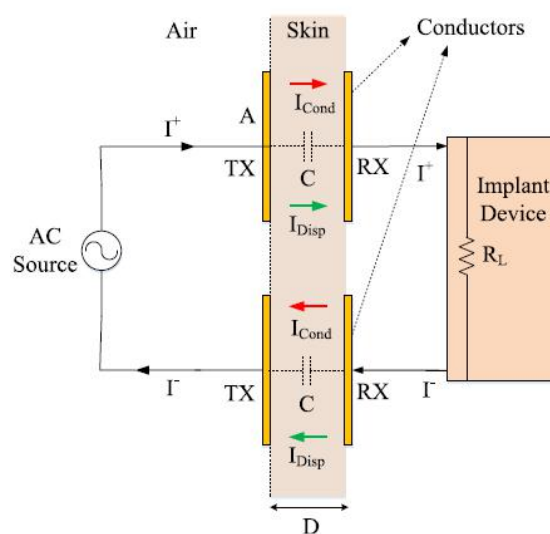


Figure 8. Near-field capacitive coupling WPT [22]

The AC source provides a time-varying electric field to the conductors on the outside of the skin. This induces the displacement current  $I_{disp}$  between the conductors. Conduction currents  $I_{cond}$  through the skin and tissues are also formed, because of the electric field between the conductors, causing undesirable losses. The ratio between the displacement currents and the conduction currents needs to be increased to achieve higher PTE. The PTE is proportional to the effective area A and inversely proportional to the separating distance D.

Some factors that limit the efficiency of the capacitive link are: the high impedance created by the capacitive reactance between the transmitting and receiving sides, the extremely small separation distance D required

between the conductors, the weak capacitive coupling that occurs from the small size of the efficient area  $A$  of the conductors as well as their proper alignment.

The NCC WPT scheme was found to operate optimally in the frequency domain of MHz. Jegadeesan et al. [22], the only recent study focusing on NCC WPT for IMDs, reported the findings in Table 3:

Table 3. Near-field capacitive coupling power transfer [22]

| Dimensions (mm <sup>2</sup> ) | Power Transferred (mW) | PTE   | Optimal Frequency (MHz) |
|-------------------------------|------------------------|-------|-------------------------|
| 20*20                         | 137.8                  | 73%   | 98                      |
| 20*15                         | 125.2                  | 70%   | 138                     |
| 20*10                         | 108.4                  | 66.4% | 190                     |

To sum up, the NCC WPT scheme has provided some encouraging results for WPT as well as for data telemetry in the domain of IMDs. However, it is hampered by the extremely short separation distance between the conductive plates as well as their perfect alignment in order to achieve sufficient PTE and power transfer as well as by the high tissue losses in the form of conduction currents.

### 2.2.5 Ultrasonic Energy Transfer

The Ultrasonic Energy Transfer (UET) method makes use of ultrasound acoustic waves that propagate through the tissues in order to wirelessly deliver energy inside the human body. In order to achieve UET, an acoustic pressure wave is transmitted transcutaneously using either a piezoelectric transducer [23] or an ultrasonic oscillator [1]. A piezoelectric energy harvester that is implanted inside the body collects this AC acoustic energy of the propagating wave and converts it in electrical energy that is then rectified and converted to DC energy that can be used by the implanted device [24]. See Figure 9.

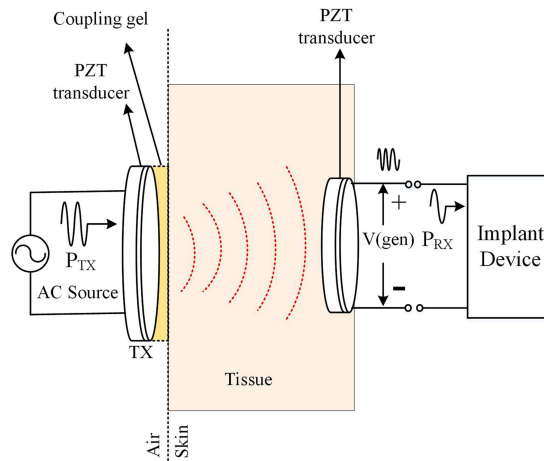


Figure 9. Schematic of UET method [1]

The PTE of the UET link depends on transducer losses, losses due to tissue absorption, losses resulting from the acoustic-impedance matching layer (the gel), the conversion losses of the receiving transducer as well as the rectifier losses. In order to maximize the PTE, Lead-Zirconate Titanate (PZT) is used to construct the ultrasonic transducers as it offers high electromechanical energy conversion efficiency. The natural focal point that lies at the border of the near and the far field of the pressure field that is generated is chosen as the preferred location for implanting the receiving transducer, as it allows the receiver to tap maximum power. The operating frequency also affects the PTE as it is connected to tissue attenuation, natural focus distance (the distance at which the natural focal point lies) and the sizes of the transducers.

The matching between the transducer and tissue acoustic impedances is also of great importance as the transferred power dramatically drops if no matching is done [1], [23], [24]. A complete block diagram of a UET link for IMDs along with all of its subsystems is depicted in Figure 10.

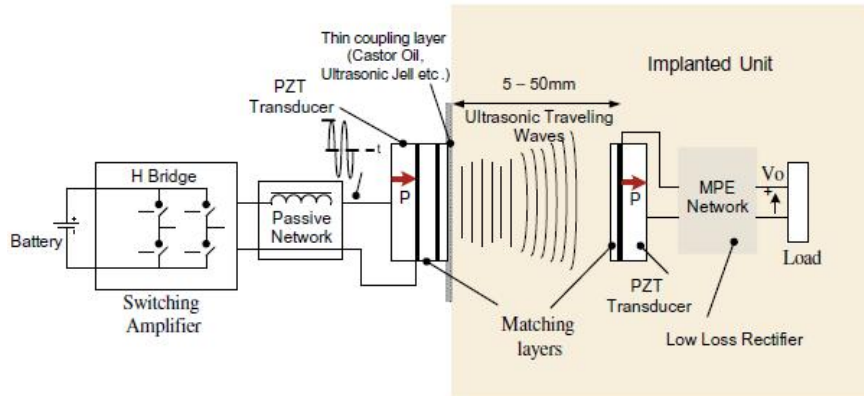


Figure 10. State of the art UET system [25]

Because of the nature of the human body and the different structure of its organs, the acoustic waves experience a large variety of acoustic impedances which result in reflection or absorption of the wave. This makes the UET scheme useful in powering devices only in specific body locations, for example locations where no bone is found between the transducer pair. Moreover, long-term effects on human tissues because of continuous ultrasound use need to be further examined.

UET also offers a limited capability of low bandwidth data transfer. In [24] the authors achieved a backward data rate of 1.2 kbit/s using ASK modulation while also achieving a power transfer of 20mW.

To sum up, UET constitutes a method that is able to transfer effectively energy to devices that are implanted up to some tens of mms inside the human body by achieving  $P_{RX}$  in the order of tens of milliwatts [26], while also offering low data transmission rates.

### 2.2.6 Far Field Wireless Power Transfer

The far-field WPT method requires the transmitting and receiving antennas to be placed at a large separation ( $R \geq \frac{2D^2}{\lambda}$ , where R is their distance, D is the largest antenna dimension and  $\lambda$  is the wavelength of the operating frequency). The transmitting antenna TX transmits electromagnetic waves. In the far-field zone, these waves become plane waves. When they reach the tuned RX antenna that is implanted inside the human body, a current is generated, that is rectified and regulated so that it can be used by the IMD [1]. Since the transferred energy is fairly low (in the order of  $\mu$ Ws) a storage unit such as a charge storage capacitor is necessary so that periodic energy supply is provided to the IMD [3], [27]. This makes the far-field WPT scheme especially useful for providing power to duty-cycle operating devices, such as sensors. A block diagram of a far-field WPT system is depicted in Figure 11, while Figure 12 depicts the energy profile of a sensor whose operation is duty cycled and makes use of far-field WPT. It is obvious that the energy provided through WPT should be greater than the energy consumption of the sensor.

The PTE of the far-field WPT method depends on the directivity of the antennas, the mismatch losses as well as the efficiency of the RF-DC conversion circuits, namely the rectifiers. Since the link operates in the domain of high frequencies, the rectification losses are fairly high. The transmitting antennas can be electrically large since they are placed outside the human body and are optimized in the free space. Therefore, high gain antennas with large bandwidth are used. On the other hand, the receiving antennas should be miniaturized and hence are electrically small, have low bandwidth and low gain and should be optimized for the conditions inside the human body. Beam focusing, parasitic patches over the human body

[28] and antenna-array techniques can help increase the received power, reduce tissue losses and increase the PTE of the system [1].

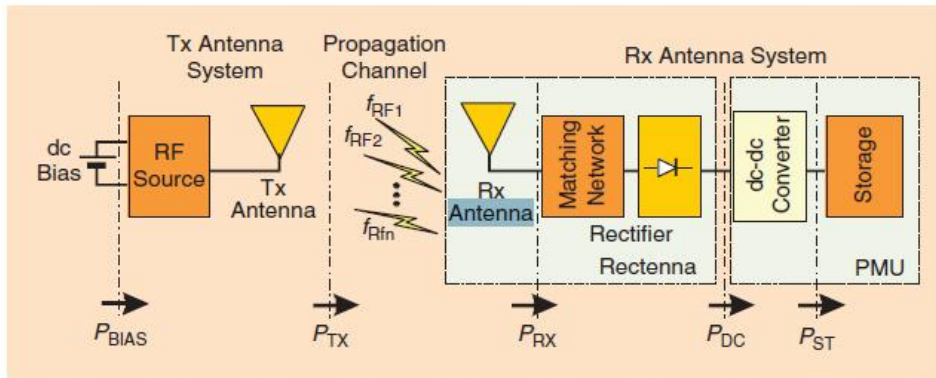


Figure 11. Far-field WPT Scheme [27]

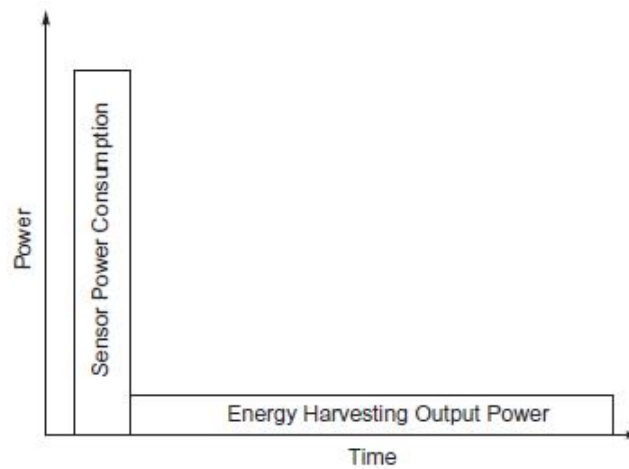


Figure 12. Energy profile of a sensor with duty cycle operation and a far-field WPT scheme [3]

Far-field WPT is suitable for long-range wireless power transfer in the Wireless Sensor Network (WSN) area of applications. Some examples are: smart houses, smart grids, Internet of Things and Wireless Body Area Networks (WBANs). Especially the field of WBANs has gained significant importance due to the need for continuous monitoring of the parameters of the human body [6]. However, since the energy transferred is fairly low, far-field WPT is still fairly inefficient in continuously and effectively powering IMDs [1].

### 2.2.7 Comparison of Wireless Power Transfer Methods

Taking everything into account, the position and size of the implants inside the body, the type of medium through which the transmission of wireless power occurs, the power budget, the functionality of the implants themselves, the WPT range as well as the dimensions of the receiver determine the WPT scheme that can be used in each occasion. Most neural implants require power at the levels of tens of mWs and therefore can be powered only via the inductive link method, since it has proven to be the most reliable method to transfer such amounts of power that also has the ability to transfer adequate amounts of data.

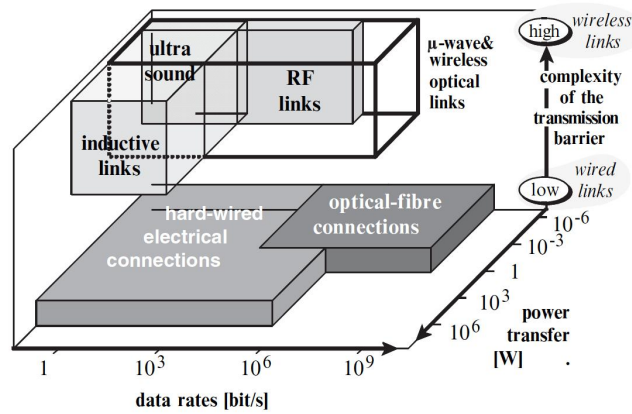


Figure 13. Power transfer capability, data rates and complexity of the transmission barrier comparison

From the aforementioned analysis and also from Figure 13 it can be concluded that the NRIC method is able to meet the power requirements of most of today's implantable devices. Similar amounts of power can be transferred by the NCC method for small separation as well as a large surface of the capacitor plates, which makes them inadequate regarding the contemporary IMD standards. Ultrasound is also able to transfer tens of mWs of power up to a few cms of transmitter-receiver separation in specific cases of IMDs. As far as far-field WPT method is concerned, it is capable of delivering minimal amounts of power in deeply placed microsystems.

As far as data telemetry is concerned, far-field as well as capacitive coupling schemes are able to achieve high data rates, while inductive coupling and ultrasound are limited to low data rates. The ability to transfer power as well as data through the same link is possible in the NRIC and NCC schemes. Ultrasound has also been reported of being able to use the same link for power and low data transfer. Far-field is mostly used for data telemetry of low-power sensors and not for the powering of IMDs.

## 2.3 Data Modulation

As was mentioned earlier, the ability to have bi-directional communication with the implanted device in order to adjust the treatment parameters, monitor the device integrity and performance and possibly run updates on the software of the implanted device is of great importance. Depending on the application, uplink and downlink transmission rates may range from some kbps to tens of Mbps [18]. For example, neural recording demands several tens of Mbps for uplink while applications such as artificial vision via retinal implants with numerous stimulation channels demand tens of Mbps in downlink [29]. Full-duplex mode (simultaneous forward and backward communication) is especially desirable. Apart from downlink/uplink, data telemetry can be further discriminated in active/passive, carrier/pulse and multi-/single-carrier based techniques.

Digital data modulation is used in order to impose the data on a high frequency carrier signal, usually a sinusoid by altering a parameter of this carrier signal. Thus, signal transmission takes place by modulating different parameters like amplitude, phase or frequency of the signal. The criteria for choosing the "correct" modulation scheme vary and depend on power, bandwidth and system efficiency [30]. However, the tissue absorption poses limitations in increasing the frequency above certain levels. The most common digital modulation techniques used for wireless data transfer are single carrier and are the following: amplitude shift keying (ASK), frequency shift keying (FSK) and phase shift keying (PSK). However, modulation techniques that either combine or constitute improved versions of the aforementioned basic methods, such as QAM, QPSK and DPSK have also been proposed to achieve higher data rates [31].

The basic 3 methods of modulation are depicted in Figure 14 in their simplest form, namely in their binary form, where only 2 bits of information can be encoded in the signal, binary 1 and binary 0. In the following chapters we are going to explain the basics of these methods as well as focus on their demodulation

methods. The modulation techniques are also briefly presented, since the application we are aiming for incorporates has both uplink and downlink communication.

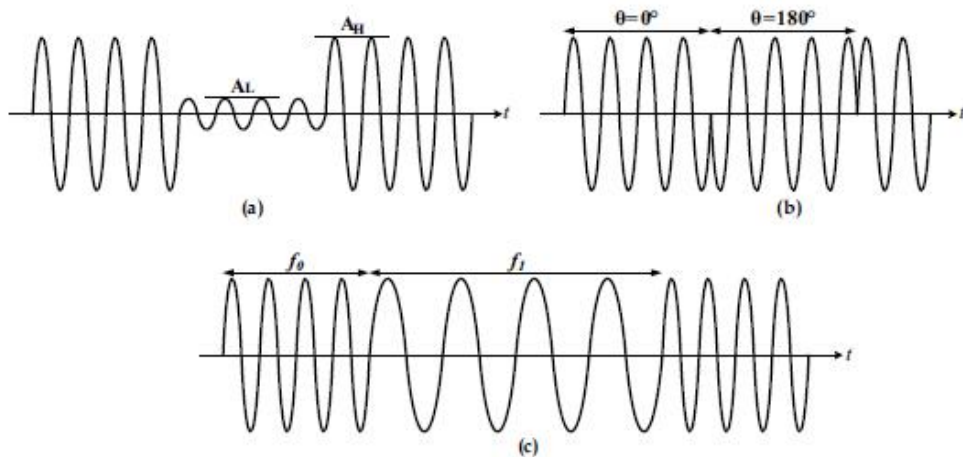


Figure 14. Binary digital modulation schemes: (a) ASK, (b) PSK and (c) FSK [9]

If one wanted to take these modulation techniques a step further, they could add multiple bits per symbol, thus allowing more information to be transferred from the carrier wave [32]. This is depicted in Figure 15, where M states the different number of amplitudes, frequencies and phases that can be achieved and therefore the number of different bits that can be encoded in the transmitted carrier. This of course increases the complexity and the power needs of the transmitting as well as the receiving circuitry.

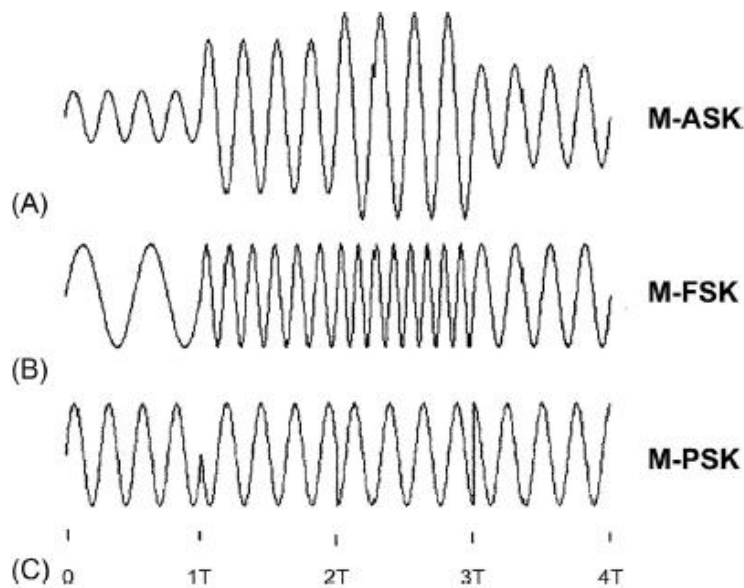


Figure 15. M-ary modulation. (A) M-ASK, (B) M-FSK, (C) M-PSK [32].

### 2.3.1 Amplitude Shift Keying

As far as binary ASK is concerned, two levels of carrier amplitude ( $A_H$  and  $A_L$ ) are used in order to represent the bits 1 and 0. These amplitude levels should be sufficiently distinguishable from the demodulation system. A measure called the Modulation index/depth is used to measure the distinction between these two amplitude levels:

$$m = \frac{A_H - A_L}{A_H} * 100\% \quad (8)$$

It can be easily understood that ASK is highly susceptible to noise, since it is highly dependable on the correct choice of amplitude levels as well as the efficiency of the detection circuits [9], [29]. The extreme case for ASK would be to increase the modulation index to 100%, namely having  $A_L=0$ . This is also known as On-Off Keying (OOK) and has the best behaviour with respect to noise, since no energy is spent on the logical 0. However, transmitting a zero-power logical 0 deteriorates the effectiveness of a wirelessly powered defence module in terms of power transfer. This occurs, because when transmitting a logical 0 without transmitting anything, no power is delivered to the device. ASK can be used in a special method for passive reverse data telemetry, also known as Load Shift Keying (LSK) or Backscattering. This method makes use of the same link that is used for forward telemetry by changing the impedance of the load. The backward data is detected from the current flowing through the transmitter, which constitutes ASK modulation on the energy transferred through the link. ASK constitutes the most common downlink method, due to its simplicity [29].

The implementation of binary ASK (OOK more specifically) modulation is represented in Figure 16. The carrier generator, that can be a voltage controlled oscillator (VCO) or a signal generator, generates a high frequency carrier. The binary sequence (message) turns the switch on and off, thus allowing and blocking the carrier wave from being transmitted. In this way a modulation index of 100% is achieved. The simple switch can also be replaced by more sophisticated circuitry that will allow lower a modulation index than 100%, that is the case in OOK. One can even achieve multiple (M) amplitudes and achieve M -ary ASK modulation.

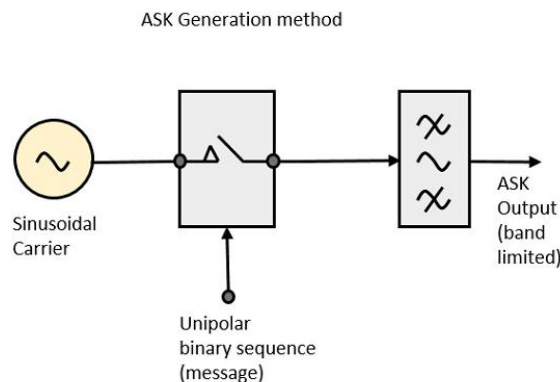


Figure 16. OOK modulation<sup>iii</sup>

As far as ASK demodulation is concerned, a simple block diagram of an asynchronous -asynchronous means that there is no need for a local carrier of the same frequency as the carrier of the modulated signal- ASK Demodulator is presented in Figure 17. As can be seen from the block diagram, the modulated signal is firstly rectifier. Then envelope detection takes place as the low-pass filter (LPF) suppresses the higher frequencies where the carrier lies. Finally, the comparator delivers the digital signal.

<sup>iii</sup> Retrieved from [https://www.tutorialspoint.com/digital\\_communication/digital\\_communication\\_amplitude\\_shift\\_keying.htm](https://www.tutorialspoint.com/digital_communication/digital_communication_amplitude_shift_keying.htm)

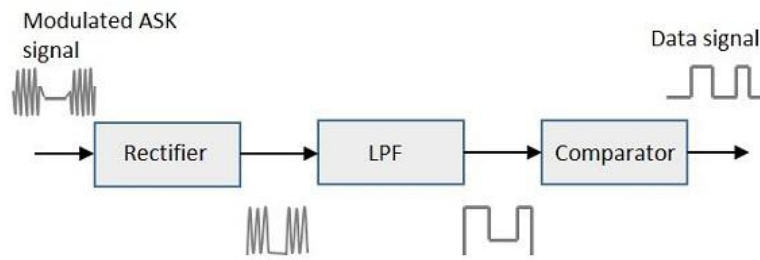


Figure 17. Asynchronous ASK demodulator<sup>iv</sup>

Synchronous ASK demodulation is another alternative and makes use of down conversion.

Most ASK demodulators make use of envelope detection using passive RC components for the low pass filter realization, which limits the achieved data rates as well as increases the chip size. Moreover, demodulators are usually unable to discriminate when a low modulation index is used and therefore opt for high indexes, in some cases they even use a 100% modulation index (OOK), which results in a poor PTE.

Regarding the state of the art implementations, in [31] the authors proposed an ASK demodulator that does not make use of RC components and is destined for full integration in IMDs. This demodulator has a low power consumption of 336 $\mu$ W and can achieve detection of a carrier with a modulation index of as low as 5.5%. In [33] the authors designed a digital ASK demodulator comprising of a Schmitt trigger, a comparator and three D-flip-flops that is able to work on various modulation indexes, with the lowest being 2.86% and 50% modulation rate. In [34] a new structure for data and clock recovery dedicated for IMDs is proposed. It consists of a fully integrated ASK demodulator along with a digital Manchester encoder. This system achieved 1Mbps data rate at a carrier frequency of 10MHz while using a modulation index of 80%. In [35] a versatile low-power ASK demodulating circuit was implemented that was meant for inductive links. It achieved a data rate of some hundreds of kbps, while the carrier's frequency ranged from 1 to 15 MHz and its modulation index could go as low as 10%, while consuming just 60 $\mu$ W of power.

### 2.3.2 Frequency Shift Keying

Frequency shift keying encodes the data in a high frequency carrier by introducing different frequencies that represent different pieces of information. The simplest form of FSK is the binary FSK modulation scheme that makes use of two different carrier frequencies:  $f_1$  and  $f_0$  (Sometimes  $f_0=2f_1$ ) in order to transmit the logic 1 and 0 levels. Therefore, the minimum bit-time is  $1/f_1$  (supposing that  $f_1$  is the lowest of the 2 frequencies). The frequencies that correspond to the logic 1 and 0 are called Mark and Space. It is worth noting that both carrier frequencies have a fixed phase at the start of each bit-time. The receiver side detects the data bits through the period of each received carrier cycle. However, in cases where the NRIC scheme is used, the link is optimized for a specific frequency and therefore the PTE may drop dramatically when a signal of another frequency is being transmitted.

Binary frequency shift keying modulation is depicted in Figure 18. Bits of information 1 and 0 are encoded in the different frequencies  $f_1$  and  $f_2$  created by their respective VCOs. A more complex decision circuit and more frequencies can also create M -ary FSK modulation where more bits can be represented by different frequencies.

<sup>iv</sup> Retrieved from [https://www.tutorialspoint.com/digital\\_communication/digital\\_communication\\_amplitude\\_shift\\_keying.htm](https://www.tutorialspoint.com/digital_communication/digital_communication_amplitude_shift_keying.htm)

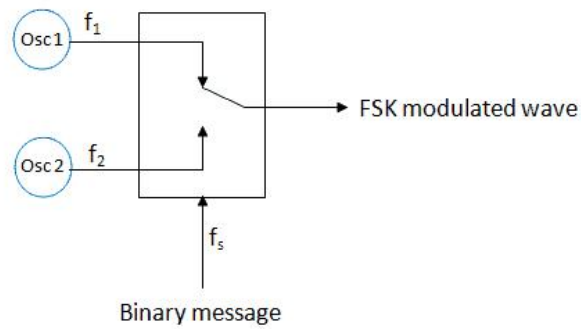


Figure 18. Binary FSK modulator<sup>v</sup>

A common FSK demodulator block diagram is depicted in Figure 19. The two bandpass filters (BPF) are tuned to the Mark and Space frequencies. The signal is then envelope-detected and compared by the decision circuit as to which one has a greater magnitude.

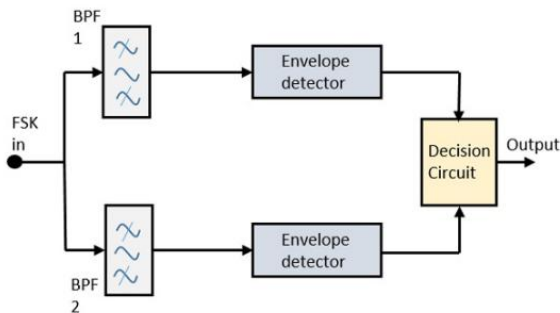


Figure 19. Asynchronous FSK demodulator<sup>vi</sup>

In synchronous FSK demodulation two mixers and two oscillators are used at the input, with each oscillator producing a carrier at one of the transmitting frequencies of Mark and Space. The signal is then filtered by LPFs and the decision circuit again determines the output depending on the measured amplitude of the signals. This is depicted in Figure 20.

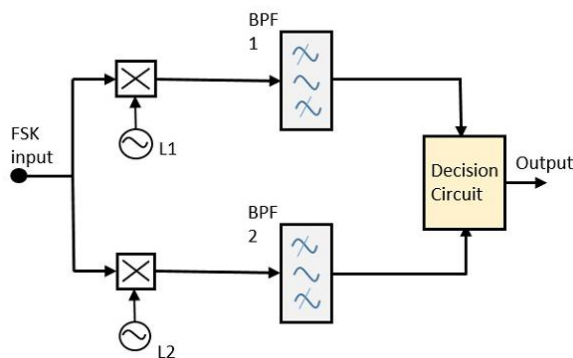


Figure 20. Synchronous FSK demodulator<sup>vii</sup>

Regarding the state of the art, in [36] the authors implemented a low power FSK modulator meant for uplink communication in an inductive link scenario for biomedical implants that is tunable to frequencies ranging

<sup>v</sup> Retrieved from <https://electronicspost.com/frequency-shift-keying-fsk/>

<sup>vi</sup> Retrieved from [https://www.tutorialspoint.com/digital\\_communication/digital\\_communication\\_amplitude\\_shift\\_keying.htm](https://www.tutorialspoint.com/digital_communication/digital_communication_amplitude_shift_keying.htm)

<sup>vii</sup> Retrieved from [https://www.tutorialspoint.com/digital\\_communication/digital\\_communication\\_amplitude\\_shift\\_keying.htm](https://www.tutorialspoint.com/digital_communication/digital_communication_amplitude_shift_keying.htm)

from 5 to tens of MHz and can also be adapted to achieve various data rates, from 450 kbps to several Mbps. In [37] a digital FSK demodulator for inductively powered IMDs was designed. Power and data are separated in two links. A data rate of 2.083Mbps was achieved with zero BER while receiving a 4.17/6.25MHz FSK carrier that was synchronized with the 2.083MHz clock. The clock was derived from the power carrier. The authors of [38] propose 3 high data-rate FSK demodulator implementations for inductively powered IMDs that require data rates higher than 1Mbps. In one of the three cases, the demodulator achieved 2.5Mbps data rate with a BER of around  $10^{-5}$ . The frequency of the carrier signal was 5/10 MHz. In [39] the authors designed an RF transceiver that receives data via FSK and communicates data back to the reader through OOK modulation through FSK-to-ASK conversion using the ISM frequency range of 902-928 MHz for WBAN applications. The transceiver achieved data rates of 8Mbps at the receiving and 100kbps at the transmitting side while consuming 639 and 0.2 $\mu$ W respectively. In [40] a SoC meant for wireless recording is proposed. This SoC makes use of a 915MHz FSK/OOK transmitter that is based on PLLs. It achieves data rates of up to 1.5Mbps. In [41] a high-performance transmitter as well as a low-power receiver that work in the ISM band are introduced. FSK is used as the received modulation scheme while OOK is used in order to transmit data back to the reader. Data rates of 20Mbps and 2Mbps were achieved while consuming 0.084nJ/b.

### 2.3.3 Phase Shift Keying

Phase Shift Keying modulation uses constant amplitude symbols as well as a fixed carrier frequency. The phase of the carrier signal is changed by varying the sine and cosine inputs at a particular time. Binary PSK (BPSK) constitutes the simplest form of PSK. Similarly to ASK and FSK, PSK can also be used to transfer more information, depending on the change in phase where more bits can be encoded at the expense of higher noise and therefore the requirement of more sophisticated detection circuits. For example, the 8-PSK scheme uses a phase shift of 45 degrees and can allow for the transmission of 3 bits (000 to 111). For matters of simplicity we are only going to examine the BPSK demodulation, where a phase shift of 180 or 0 degrees is used to represent the binary 1 and 0 respectively.

An example of a BPSK modulator is depicted in Figure 21. The balanced modulator changes the phase of the carrier by 180° according to the binary data sequence. M-ary PSK methods such as quadrature PSK (QPSK) make use of more sophisticated phase shifters instead of the balanced modulator.

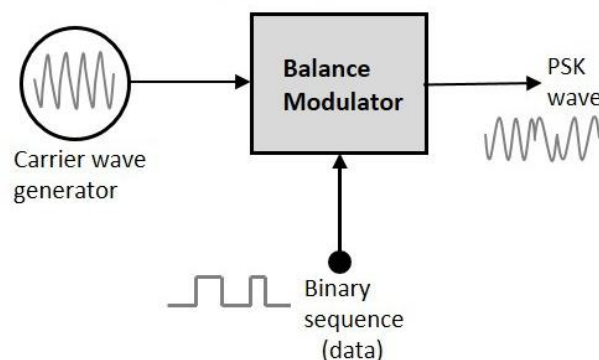


Figure 21. Binary PSK modulator<sup>viii</sup>

The demodulation process of a BPSK modulated signal is achieved by the so-called COSTAS loop demodulator depicted in Figure 22. It consists of two parallel phase locked loops (PLLs). The frequency of the VCO is controlled by the phase error outputs of these PLLs.  $V_{in}(t) = m(t)\sin(\omega_1 t + \theta_1)$  (9) constitutes the

<sup>viii</sup> Retrieved from [https://www.tutorialspoint.com/digital\\_communication/digital\\_communication\\_phase\\_shift\\_keying.htm](https://www.tutorialspoint.com/digital_communication/digital_communication_phase_shift_keying.htm)

input signal, where  $m(t)$  is the data stream while  $\sin(\omega_1 t + \theta_1)$  is the carrier. After being low pass filtered, the upper and lower branch outputs are  $V_{OI}(t) = m(t)\cos(\theta_1 - \theta_2)$  (10),  $V_{OQ}(t) = m(t)\sin(\theta_1 - \theta_2)$  (11). In the central branch there is a loop filter and an additional multiplier making the Voltage of the VCO  $V_M(t) = \frac{1}{2}m^2(t)\sin 2(\theta_1 - \theta_2)$  (12). It can be clearly seen that the control signal is made proportional only to the phase difference by the square term of the data stream, as is the case in the simple PLL loop. In the locked state of the PLL the phases  $\theta_1$  and  $\theta_2$  are almost identical. In this way, the output of the upper branch  $V_{OI}$  becomes the demodulated signal. COSTAS loops sometimes experience a situation called phase ambiguity. This is caused by the lack of phase synchronization between the transmitter and the local oscillator.

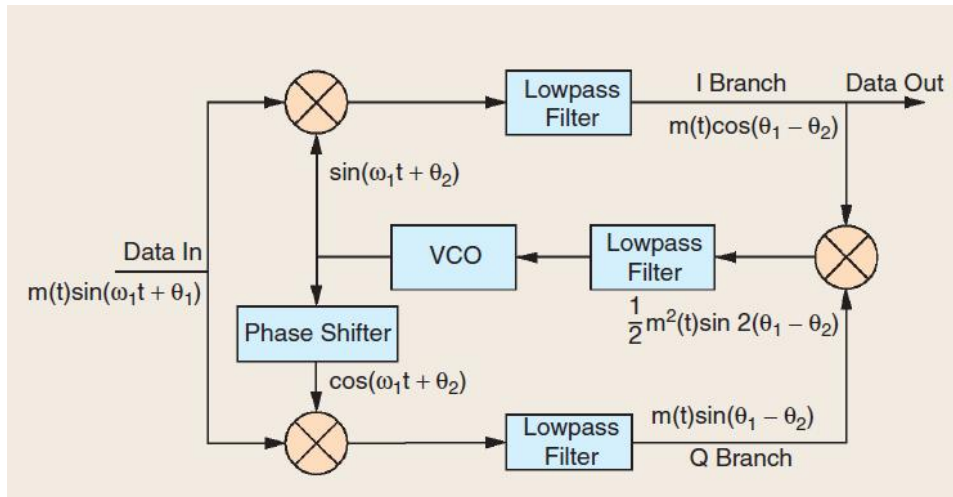


Figure 22. COSTAS loop BPSK demodulator [29]

As far as the state of the art regarding PSK modulation/demodulation is concerned, in [42] a BPSK transceiver for downlink (modulator and demodulator) and a multilevel LSK transceiver for uplink communication that achieves 2-bit combinations (00, 01, 10, 11) are designed. Operating at a 13.56MHz carrier frequency, a downlink data rate of 100kbps is achieved, while the four 2-bit combinations using LSK could be effectively produced. In [43], the authors achieve a bit rate of 20kbps at 13.56MHz using BPSK, while, in [44], a fully integrated differential PSK (DPSK) demodulator for a dual-band telemetry wireless inductive link is designed that operates at a 22MHz carrier frequency providing data rates of up to 4 Mbps. In [45], a low-power QPSK modulator for uplink is proposed that achieves a data rate of 2Mbps at a carrier frequency of 12.5MHz. In [46], a fully integrated low-power BPSK demodulator based on a hard-limited COSTAS loop topology is proposed. It achieves a transmission rate of 1.12Mbps, uses less 0.7mW power at a voltage of 1.8V. In [47], the authors implement an inductive link comprising 6 coils (2 for power, 2 for the downlink and 2 for the uplink telemetry). They use the offset quadrature PSK (OQPSK) data telemetry scheme and achieve a data rate of 4.16 Mbps with a BER of less than  $2 \times 10^{-6}$ .

### 2.3.4 Comparison of Data Modulation Techniques

Taking everything into account, ASK is achieved via simple modulation and demodulation circuits, but has the drawbacks of low data rate transmission and high sensitivity to noise as well as inaccuracies in the synchronization between data and clock signals [9], [18]. In BFSK two different carrier frequencies are used, with the data rate being limited to the lower frequency. Compared to ASK, FSK and PSK experiences less interference, but usually requires PLLs for coherent demodulation [17], which heavily increases the power budget of the receiver. Carrier-based modulation is a very power-demanding process and should therefore be rejected for uplink communications in the case of IMDs, where the expected lifetime of the devices should be substantially high, leaving speed-limited modulations such as LSK as one of the few options for

passive uplink communication [29], [18]. This limited data rate for uplink would be acceptable in our ZPD scenario, where it simply serves to establish trust between the IMD and the reader and the “normal” communication is then handled by the IMD instead of the ZPD module.

### 2.3.5 Research Questions

Having concluded the literature research, the research question is the following: Is there a way to create an analog circuit module that employs wireless power transfer as well as data transfer that can serve as a ZPD module and ensure BDoS protection? Furthermore, can this analog circuit be achieved using minimal space in order for it to be used as a security add-on in commercial implants?

# 3 System Overview

## 3.1 System Description

As was mentioned earlier, this thesis is aiming for a security solution against the Denial of Battery Service attack that can be incorporated in a large category of commercial implants. This means that the “target group” is going to be implants that have wireless connectivity with an outside reader. The power transferred via this communication should be sufficient to drive our module, which is going to decide whether the reader should be allowed to communicate with the implant or not, without depleting the IMD’s battery at all. This is going to be achieved by the execution of a cryptographically strong communication protocol using a bidirectional “handshake” from both parties, designed by the Neuroscience department of the Erasmus Medical Centre in Rotterdam. Therefore, the system we are designing has to incorporate a micro-controller that is programmed to execute this handshake between the reader and the module. It is going to examine the received data from the reader and decide whether the entity trying to communicate with the implanted device should be authorized to do so. This decision will be related back to the reader. The system-level block diagram is depicted in Figure 23.

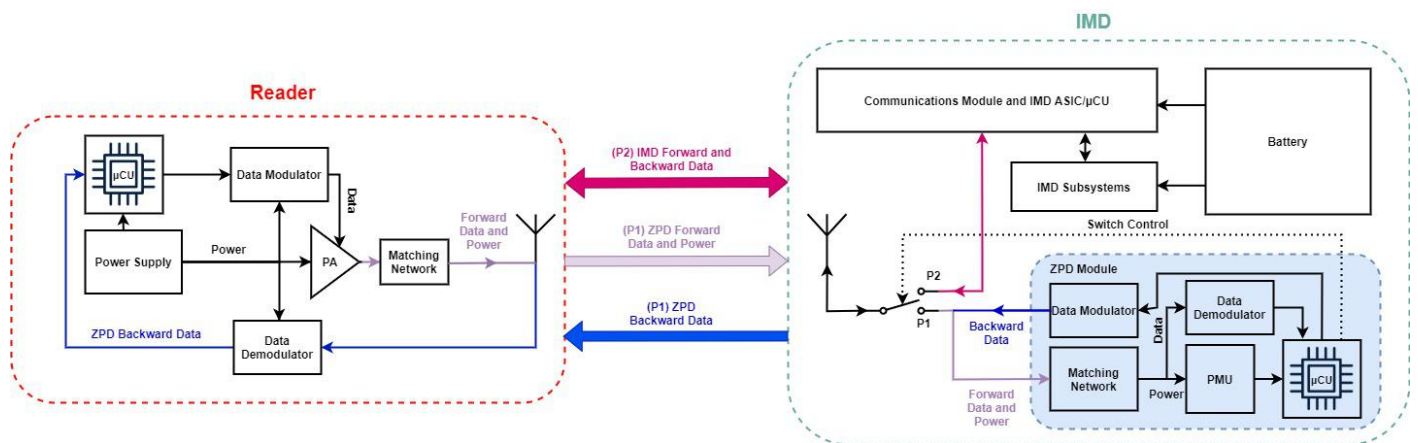


Figure 23. Proposed system-level block diagram

In this figure, one can observe the functional blocks of the whole system as well as of the desired ZPD module, highlighted in light blue. It can be seen that data and power will be transmitted from the reader in order to both power the ZPD module as well as provide its micro-controller unit with the information needed for the verification of the user that is trying to communicate with the IMD. Depending on the information received, the module is going to reach a decision and relay it back to the reader through the backward data channel, or require more information for the verification process .

The reader is located outside of the human body. Since it has to provide both power and data, it consists of a Power Amplifier and Matching Network to generate the power required by the ZPD module as well as a data modulator for the forward data telemetry that is controlled by a micro-controller/processor ( $\mu$ CU). The final part of the reader will be a data demodulator meant for the demodulation of the backward data sent by the module, that will then be processed by the controller/processor.

The module itself is meant to require minimal space so that it can be incorporated in the IMD as an add-on. The exact location cannot be specified, because it will vary from device to device. For example, there are implants that use antennas outside of the titanium encapsulation and are covered by biocompatible silicone layer or titanium alloys with low resistivity (St. Jude’s ANS Rechargeable Spinal Cord Stimulators Eon and

Eon Mini<sup>ix</sup>). The ZPD module could be placed just underneath that plastic layer and make use of the antenna of the device itself. Another alternative would be to place the module in the lead strain relief of IMDs that make use of leads, such as neurostimulators, defibrilators and pacemakers. If the antenna of the IMD does not meet the requirements for data and power transfer the module could incorporate an antenna of its own, which of course would increase the area required by the device. One could also argue that the leads of such IMDs could be used as antennas to transfer information and possibly power to the module. Finally, the module should have control over the communication link in order to make the decision of granting or denying access.

The ZPD module itself will consist of a Power Management Unit that will include a rectifier and a charge storage capacitor in order to harvest the power sent by the reader. A matching network may be used in order to increase the power transfer efficiency if needed. As far as the data is concerned, a demodulator will decode the data and feed them to the micro-controller unit of the module. Depending on the received data, the module will take the decision to either allow or completely block the communication between the reader and the IMD, which is depicted by a switch.

## 3.2 System Characteristics

As a proof of concept we are going to design a transmitter as well as a receiver in order to achieve wireless power and data transfer by using off-the-shelf discrete components. The aim is to have a system that:

- Achieves good power efficiency and sufficient power transfer.
- Reliably transmits and receives information over small distances.
- Consists of as less components as possible so that minimum space is occupied.
- If the concept proves successful, an application-specific integrated circuit (ASIC) that implements all the parts of the module can be designed in order to further reduce the size and have all the components in one piece.

Taking these characteristics into consideration led to the decision to make use of the NRIC scheme to provide wireless power transfer, since it is able to achieve the largest amounts of power transfer over small distances. Moreover, ASK is chosen as the selected method of data modulation since it requires the simplest circuitry for both transmitting data as well as demodulating them. The building blocks of the proposed circuit and their design process are presented in the following chapter.

<sup>ix</sup>Retrieved from <http://www.implantable-device.com/2012/01/12/st-judes-ans-rechargeable-spinal-cord-stimulators-eon-and-eon-mini/>

# 4 Circuit Design

## 4.1 Transmitter

As was mentioned earlier, the transmitter consists of a transmitting coil, a power amplifier, an ASK modulator as well as an ASK demodulator. The frequency of operation for the wireless power transfer is the 13.56MHz band, which is a very common industrial, scientific and medical frequency band (ISM).

### 4.1.1 Antenna

Since it is desired to implement both power and data transfer, a coil that can handle both tasks adequately was needed. We were lucky to be allowed to make use of a coil designed and manufactured by Salvia Bioelectronics, a company that is active in the field of bioelectronics<sup>x</sup>. The inductance of this coil is around 1.5uH, with a quality factor Q around 106. For matters of simplicity the same inductor was used at the receiver side of our system. The whole design of was based on these two inductors.

After the data of the inductors were provided, the following calculations were made:

First of all, the mutual inductance of the coils was calculated as  $M = \frac{\mu_0 \mu_r N_1 N_2 A}{l} = 58.945 nH$  (13)

where  $N_1, N_2$  are the number of turns of each coil,  $A$  and  $l$  are the effective area and length of the magnetic path,  $\mu_0$  and  $\mu_r$  are the permeability of free space and the relative permeability of air respectively. Then the

coupling factor of the coils was calculated as  $k = \frac{M}{\sqrt{L_1 L_2}} \approx 0.04$  (14). In order to resonate the antenna at

the desired frequency of 13.56MHz, a capacitor has to be placed in parallel with the inductor. This capacitor was calculated as:  $C = \frac{1}{(2\pi f L)^2} \approx 95 pF$  (15).

### 4.1.2 Class-E Amplifier

In order to drive the transmitting coil, it was decided to use a Class-E high efficiency switching-mode amplifier. The choice is made because of the simplicity of the circuitry required to build these types of RF amplifiers as well as the high efficiency they are able to achieve at higher frequencies, compared to other classes such as Class-D amplifiers, by also requiring only one power switch, resulting in a single ended implementation [48], [49]. A Class-E amplifier is depicted in Figure 24.

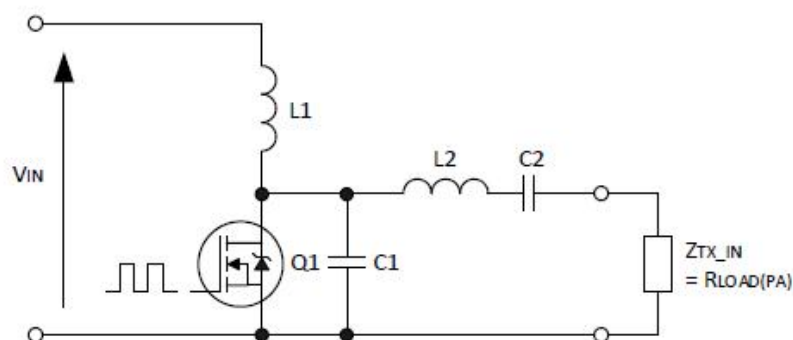


Figure 24. Class-E amplifier typical topology [51]

As far as the operation of the amplifier is concerned, it can be shortly described in the following paragraph.

<sup>x</sup>Retrieved from <https://www.salvianeuro.com/>

The transistor acts as a power switch, driven by the driver at its gate (or base) with a frequency  $f_{sw}$ . By turning on and off at  $f_{sw}$ , the DC energy provided by the power supply is converted into AC energy at the same switching frequency  $f_{sw}$ . Maximum output is obtained by setting the duty rate of the switching signal at 50 percent. The voltage and current waveforms of the Class-E amplifier's operation are depicted in Figure 25.

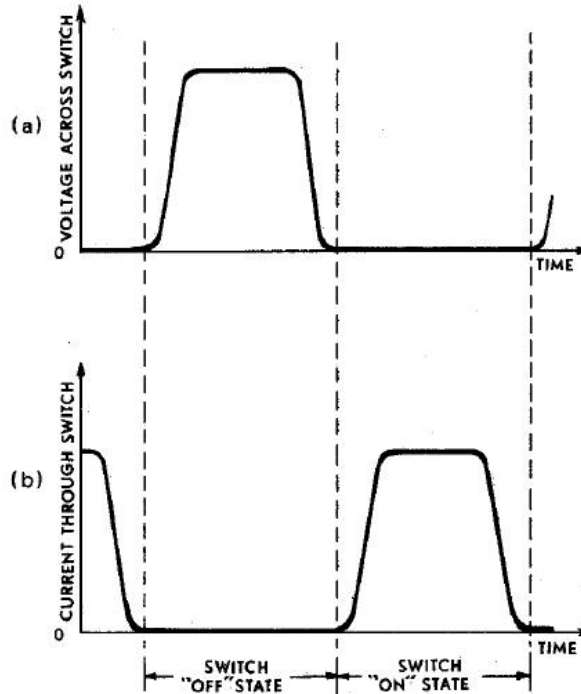


Figure 25. Ideal waveforms of class-E amplifier operation for maximum power efficiency. (a) Voltage across the switch. (b) Current through the switch [48]

During the on-state the voltage is very low while a large current is flowing, which means the transistor is working as a low-resistance closed switch. During the off-state almost no current flows, while the voltage is high. In this case the transistor acts as an open switch. This operation ensures that there is never a high voltage and a high current at the same time. Hence, the losses associated with the transistor are low.

To sum up, for optimum operation of the class-E amplifier, three conditions need to be met:

- The voltage rise of the transistor at turn-off should be delayed until after the current has returned to zero.
- The transistor voltage should be zero before the turn-on time, when the current begins to rise.
- The slope of the drain voltage should be zero at the turn-on time.

In order to achieve high efficiency, the Class-E amplifier makes use of a non-resistive load network, a resonating tank comprised of a capacitor in series with an inductor. This, in addition to the resonated transmitting antenna makes the impedance seen by the amplifier purely real, therefore a resistance. The Antenna then converts the electrical energy into magnetostatic energy. This is represented by the antenna resistance.

Regarding the selection of the passive components of the amplifier, the input voltage at inductor  $L_1$  must be able to provide a roughly constant current to the circuit and thus needs to be large enough. This current will have some ripple, depending on the value of the inductance, but the average will be equal to the DC input current. This current is sunk to the ground when the switch ( $Q_1$ ) is on. When the switch is off, the current flows into the network of capacitors and inductors ( $C_1, C_{oss}, L_2$ ) which is designed to have purely resistive

behaviour, thus building up a voltage at the equivalent resistance. The minimum value of  $L_1$  can be calculated by:

$$L_{1\min} = \frac{(\pi^2 + 4)R_{LOAD(PA)}}{f_{sw}} \approx 1.128\mu H \quad (16),$$

since  $R_{LOAD(PA)} = Z_{TX\_IN}(\omega_{res}) \approx 1.1025\Omega$  and  $f_{sw} = 13.56MHz$ . The chosen inductance was  $L_1 = 3.3\mu H$

The amplifier circuit has two resonant frequencies: one when the switch is closed, where  $C_1$  and the output capacitance of the transistor,  $C_{oss}$ , are shorted and another when the switch is open, thus including both aforementioned capacitances. The frequencies are given by the following equations:

$$f_{r1} = \frac{1}{2\pi\sqrt{L_2C_2}} \quad (17), \quad f_{r2} = \frac{1}{2\pi\sqrt{L_2C_{eq}}} \quad (18), \quad \text{where } C_{eq} = \frac{(C_1 + C_{oss})C_2}{C_1 + C_2 + C_{oss}} \quad (19).$$

The frequencies should also satisfy the conditions:

$$\frac{1}{2f_{r1}} + \frac{1}{2f_{r2}} = \frac{1}{f_{sw}} \quad (20) \quad \text{and} \quad f_{r1} < f_{sw} < f_{r2} \quad (21).$$

After searching in the available stores for electronic components as well as after running some simulations on the LT Spice simulator the following values were selected for the components:  $C_{oss} = 30pF$ ,  $C_1 = 90pF$ ,  $C_2 = 110pF$ ,  $L_2 = 1.4\mu H$ . These give the resonating frequencies:  $f_{r1} = 12.83MHz$  and  $f_{r2} = 18.85MHz$ , that satisfy (6) and (5) by 88.87%, meaning that the left part of (5) gives a period that equals  $T_{sw} * 88.87\%$

The amplifier circuit along with the transmitter coil are depicted in Figure 26. It is noteworthy that parasitic resistances have been included in each separate component and therefore have not been added as separate elements in the circuit. The schematic was made using LT SPICE, a circuit simulator from Linear Technologies.

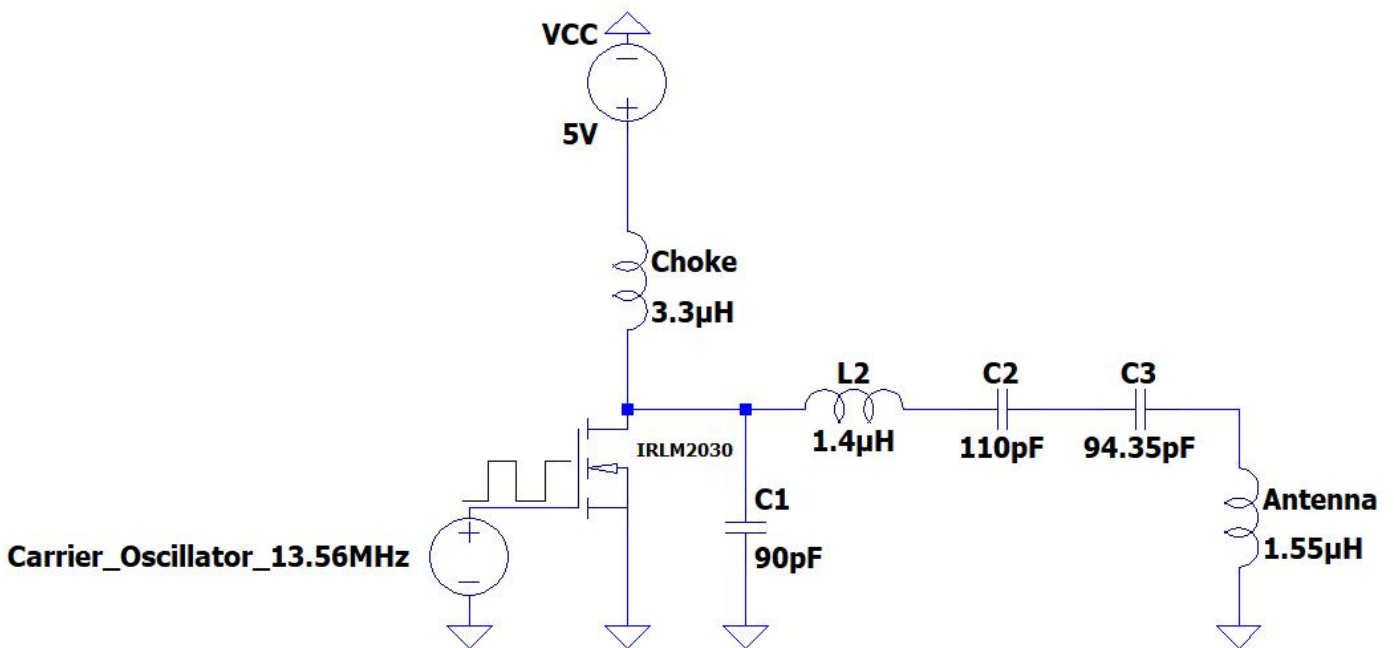


Figure 26. Class E amplifier and transmitting antenna

### 4.1.3 ASK Modulator

The amplitude modulation circuit that was chosen consists of two Bipolar Junctions Transistors (BJTs) in a Darlington Pair configuration, that control the voltage amplitude that is fed to the class E-Amplifier. An example of this configuration is depicted in Figure 27.

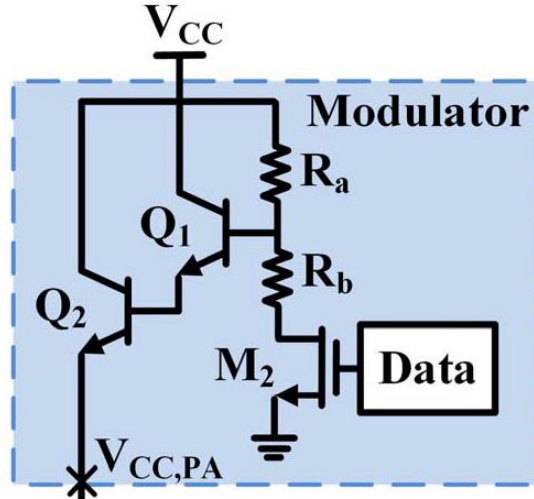


Figure 27. Data modulation and power transfer [50]

The function of this circuit is the following.

The voltage source named Data is controlled by a micro-controller or a microprocessor. It generates a binary signal turning the MOSFET  $M_2$  on and off.  $M_2$  namely works as a switch that allows current to go through the transistor to the ground, when turned on and blocks all current at the off-state. The amount of current and therefore generated voltage depends on the ratio of the resistive divider that consists of  $R_a$  and  $R_b$ . The voltage that applied to the class E amplifier can therefore be described as:  $V_{cc} - 2V_{BE}$  when  $M_2$  is

off and  $V_{cc} \frac{R_a}{R_a + R_b} - 2V_{BE}$  when  $M_2$  is on. Thus, by changing the value of the resistive divider we are able to

control the amount of voltage that is “drained” from the amplifier. In this way we are able to control the modulation depth of the amplitude modulated signal. The modulation index is given by the formula:

$$MI = \frac{V_{cc} R_b}{(V_{cc} - 2V_{BE})(R_a + R_b)} \quad (22)$$

It can be easily understood that the voltage drop caused by the two bipolar transistors constitutes one limiting factor that causes the overall power efficiency of the transmitter to drop. However, the transmitter is meant to be outside of the human body and will therefore have significantly large resources when compared to the receiver. There have been some publications aimed at ameliorating this power drop by implementing ASK modulation that is achieved by using different techniques. [50] and [51] constitute examples of different implementations.

The ASK modulator, the amplifier circuit and the transmitter coil are depicted in Figure 28. It has to be noted, that the node “Modulated\_Uplink\_Data” leads the backscattered signal to the demodulation circuit.

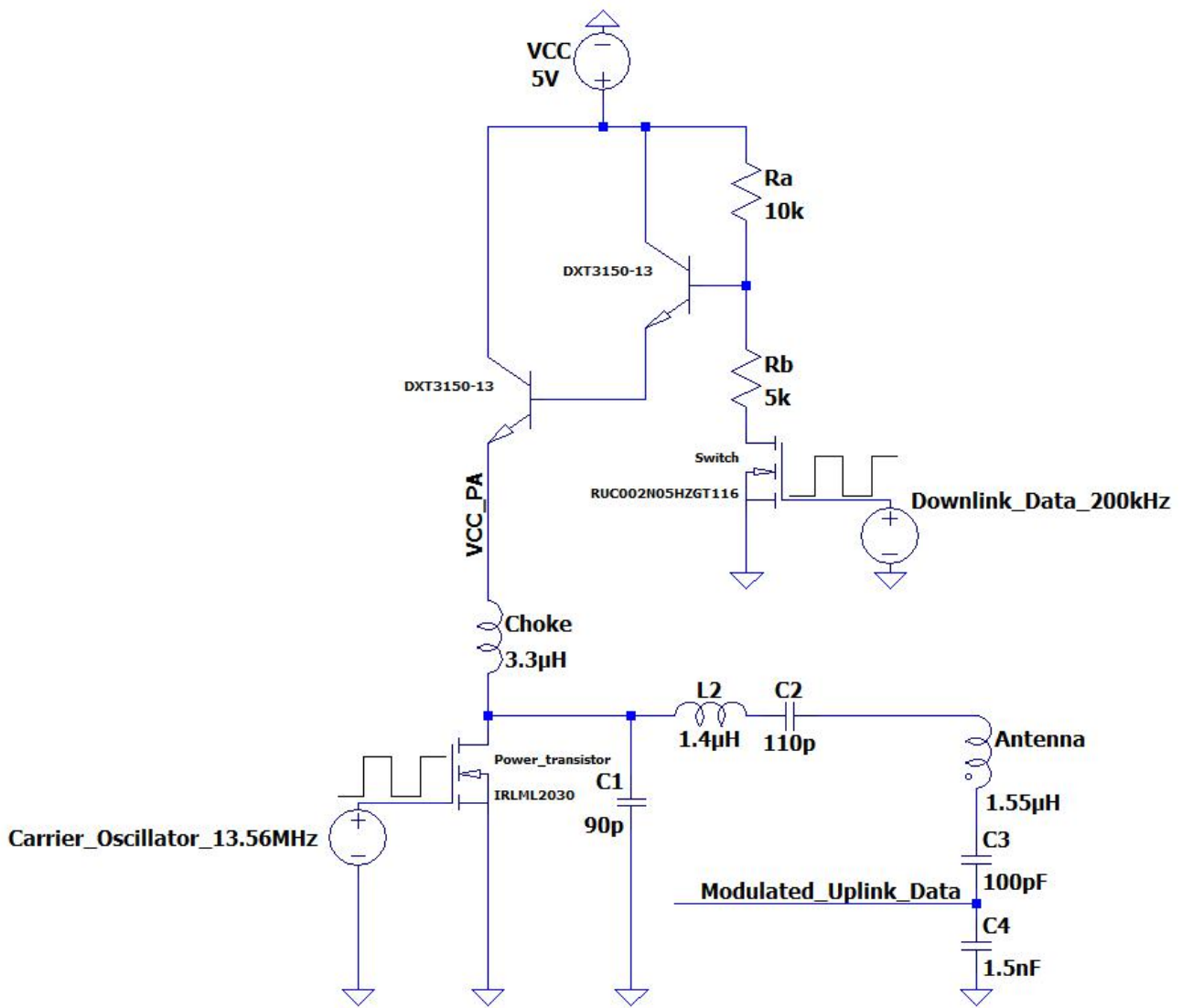


Figure 28. ASK modulator, power amplifier and transmitting coil

One can easily spot the use of a capacitive divider consisting of  $C_3$  and  $C_4$  instead of a simple capacitor in order to resonate the transmitting coil. The reason behind this is explained in the following chapter.

#### 4.1.4 ASK Demodulator

As was mentioned in the system description, the transmitting side, i.e., the reader outside of the human body, of our system should also have the ability to detect and demodulate data that the receiving side, the ZPD module on the IMD, produces through backscattering. Since backscattering (a.k.a. LSK) constitutes a special form of ASK modulation, it is only logical that an ASK demodulator is going to be placed at the transmitting side of our system in order to extract the data sent by the ZPD module.

In order to implement the data demodulator, a window comparator was chosen. The operation of the demodulator is depicted in Figure 29.

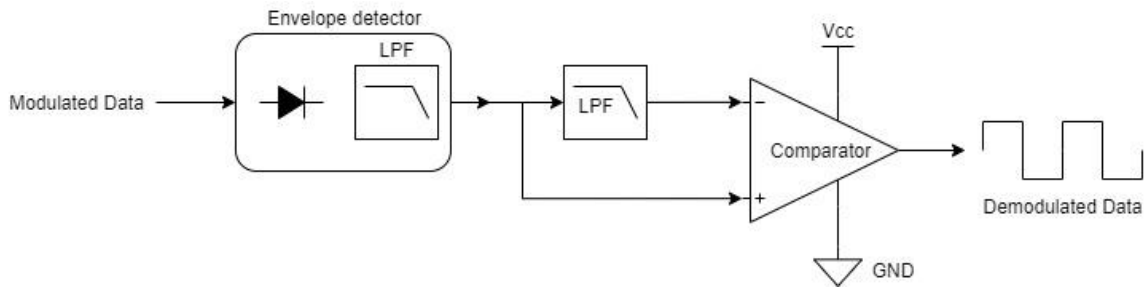


Figure 29. ASK demodulation scheme

The amplitude modulated data is received at the antenna and is passed through the envelope detector where the signal is rectified and is passed through the first LPF that is tuned for the frequency of the backscattered data. This filtered signal is fed to the positive pin of the comparator and is also passed through another LPF that has a much lower cut-off frequency. This second filter extracts the average value of the filtered signal and feeds its output to the negative pin of the comparator. The comparison of these two low pass filtered signals reproduces the signal that was received via backscattering.

The ASK demodulator implementation is depicted in Figure 30. The Schottky diode  $D_1$  along with  $R_3$  and  $C_5$  constitute the envelope detector while  $R_1$  and  $C_6$  form the LPF. Finally, operational amplifier  $U_1$  indicates the comparator of our implementation, which is a comparator with hysteresis instead of a simple operational amplifier.

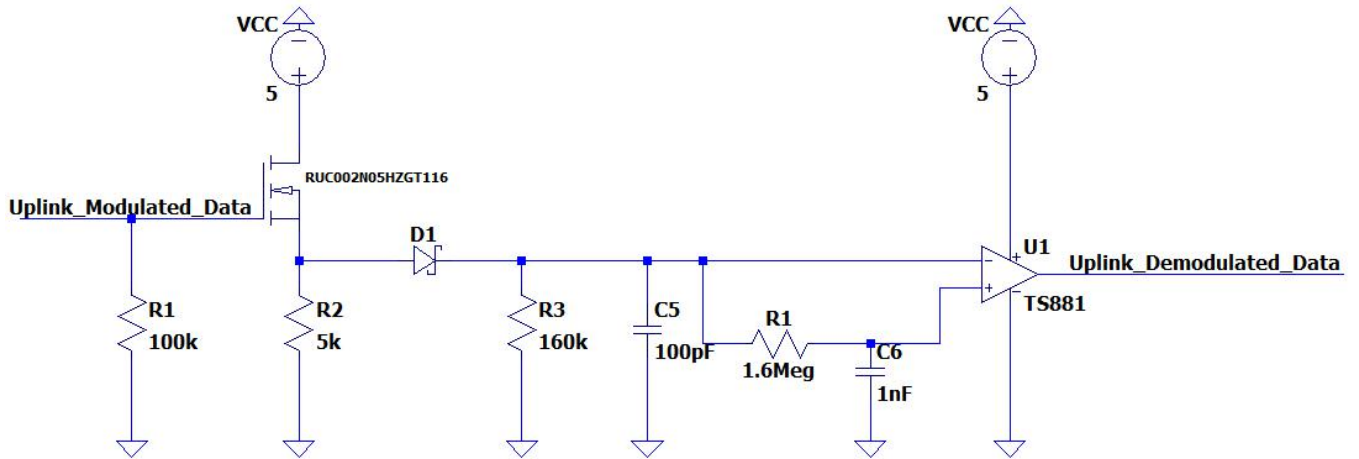


Figure 30. Uplink data demodulator

In our implementation it was chosen to have a backscattered signal of around 10kHz. Therefore the values of the filters' components were chosen as:  $R_3 = 160k\Omega$ ,  $C_5 = 100pF$ ,  $R_1 = 1.6M\Omega$ ,  $C_6 = 1nF$ , which determine

the cut off frequencies:  $f_1 = \frac{1}{2\pi R_3 C_5} \approx 10kHz$  (23),  $f_2 = \frac{1}{2\pi R_1 C_6} \approx 10Hz$  (24).

The OUT node is the same as the one depicted in Figure 31. The equations derived from the capacitive divider are the following:  $X_{C_3} = \frac{1}{2\pi f C_3}$  (25),  $X_{C_5} = \frac{1}{2\pi f C_4}$  (26). Therefore, the voltage that at the

"Modulated\_Data" node is  $V_{Uplink\_Data} = \frac{X_{C_4}}{X_{C_4} + X_{C_3}} V_{OUT} = \frac{C_3}{C_3 + C_4} V_{OUT}$  (27)

The use of the capacitive divider is essential since the voltage at the coil is expected to be significantly large. This would compromise the operation of the comparator, since it would need a very high positive voltage so that it would not saturate and would continue to work as intended. Thus, by the use of the capacitive divider we are able to not only resonate the transmitting coil, but also to provide the demodulation circuit with a low enough voltage that allows its smooth operation. In order to achieve a capacitance that not only achieves resonance for the coil, but also proper voltage division, it is chosen to use capacitors with the following values:  $C_3 = 100\text{pF}$ ,  $C_4 = 1.5\text{nF}$ . In this way, the voltage is lowered by a factor of  $1/16$ . It has to be noted that this ratio is a product of both simulation as well as experimentation data that are going to be presented in Chapter 6.

Another difference between our implementation and the generic one is the use of a MOSFET in Source Follower (Common Drain) topology. This transistor acts as a buffer, providing high impedance and isolating the demodulation circuit. More specifically,  $R_2$  sets the current that is drawn from  $V_{CC}$  and  $R_4$  creates a high impedance path to ground.

With the description of the demodulator, the design of the transmitter has been completed.

## 4.2 Receiver

The receiving side consists of a receiver antenna (coil), resonated at the frequency of 13.56MHz, a charge pump rectifier, designed to not only rectify the received AC signal but also boost the voltage provided to the load, a demodulator tuned at the frequency of the data rate transmitted by the reader. Finally, the receiver makes use of a backscattering circuit in order to be able to communicate data back to the transmitting side, namely the reader outside of the human body. It has to be noted that the receiver was designed to provide power to a microcontroller unit that would be designed to execute the security protocol described in [8].

As far as the requirements of the output are concerned, it was calculated that it would require at least 2 mW of power to execute the communication protocol. The voltage required by the  $\mu\text{CU}$  is between 3.3 and 3.8 volts.

### 4.2.1 Antenna

The antenna at the receiving side of our system is a coil identical to the one used at the transmitting side. The inductance of the coil is around 1.5 $\mu\text{H}$  and therefore a capacitance of around 95pF resonates the receiver at the desired frequency of 13.56MHz.

### 4.2.2 Rectifier and Storage Unit

Due to the low coupling factor of the inductors it was expected that the voltages achieved at the receiving side of the system would be fairly low and would not meet the design goals. Therefore, we decided to make use of a charge pump rectifier topology in order to boost the received voltage and reach the minimum 3.3V required by the load. A general implementation of a charge pump rectifier is depicted in Figure 31.

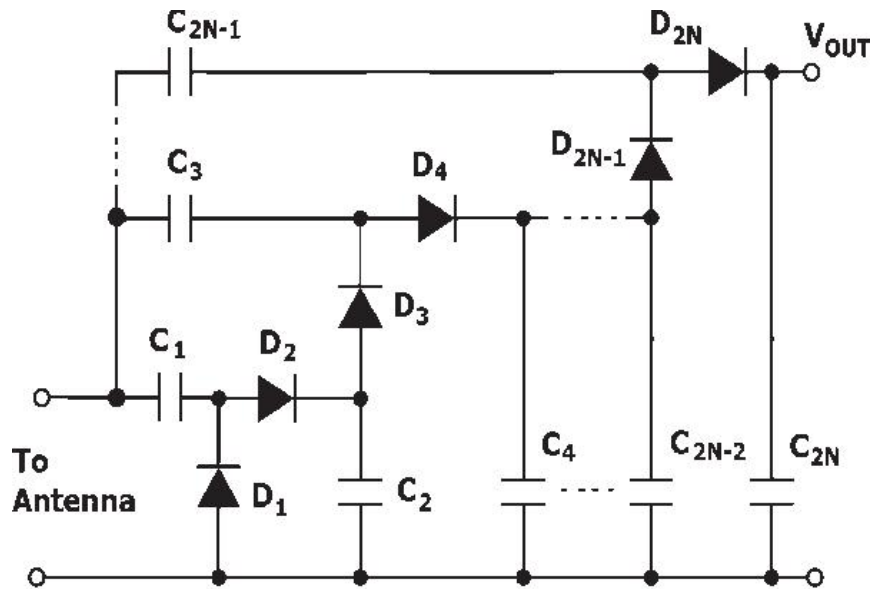


Figure 31. General charge pump rectifier topology [52]

The operation of the charge pump rectifier is fairly simple. It consists of voltage-doubling “stages”. Each stage consists of two capacitors and two diodes, i.e.  $C_1, C_2, D_1, D_2$  consists one such stage. In each stage, the negative halves of the received oscillating signal pass through the  $D_{2N-1}$  diodes and charge the capacitors  $C_{2N-1}$ . When the positive part of the signal arrives, the stored charge is released and is added to the charge delivered, effectively doubling it and thus the voltage achieved at the output of each stage.

However, the charge pump rectifier makes use of capacitors and diodes (or diode connected transistors in order to energetically storage the electric charge). These contribute to the whole capacitance “seen” by the antenna detuning it from resonance and therefore reducing the efficiency of the power transfer. This is one of the limitations and main design factors of this experimental prototype.

The choice of capacitor value for the charge pump was made based on the assumption that no more than 5V would be available from the power supply of the transmitter. After many simulations in LTSPICE, we made the decision to make use of a 3 stage charge pump rectifier with 4.7nF capacitors and Schottky diodes. These 3 stages create a voltage six times larger than the one at the input of the rectifier. This system is depicted in Figure 32.

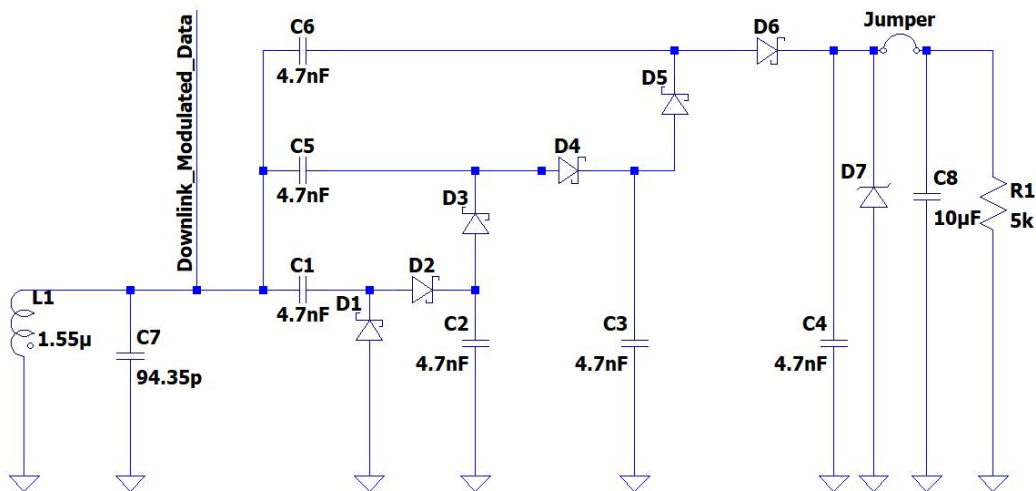


Figure 32. Receiving coil, charge pump rectifier and load schematic

In this schematic one can observe that the receiving coil  $L_1$  along with its resonating capacitor  $C_7$ , the charge pump rectifier that consists of the capacitors  $C_1$  to  $C_6$  and diodes  $D_1$  to  $D_6$ , the load, namely the  $5k\Omega$  resistor  $R_1$  as well as a capacitor  $C_8$  of  $10\mu F$  that not only acts as a storage element, but also filters the voltage ripple so that a more stable voltage is provided to the load. The output of the rectifier is disconnected from the storage element and the load. Instead of connecting them directly, jumpers were used that would allow them to connect via external wires. This allowed the possibility of introducing a voltage regulator or a power-management IC between the two nodes. Finally, the Zener diode  $D_7$  that has a reverse voltage threshold of around  $6V$  is placed in parallel with the load for overvoltage protection, since voltages above  $6V$  could harm the microcontroller.

### 4.2.3 ASK Demodulator

The implementation of the ASK demodulator at the receiving side is similar to the one at the transmitting side. The things that are different are: the cut-off frequencies of the LPFs, the absence of the buffer at the input and the use of the rectified output voltage  $V_{out}$  as supply to the comparator. The designed circuit is depicted in Figure 33.

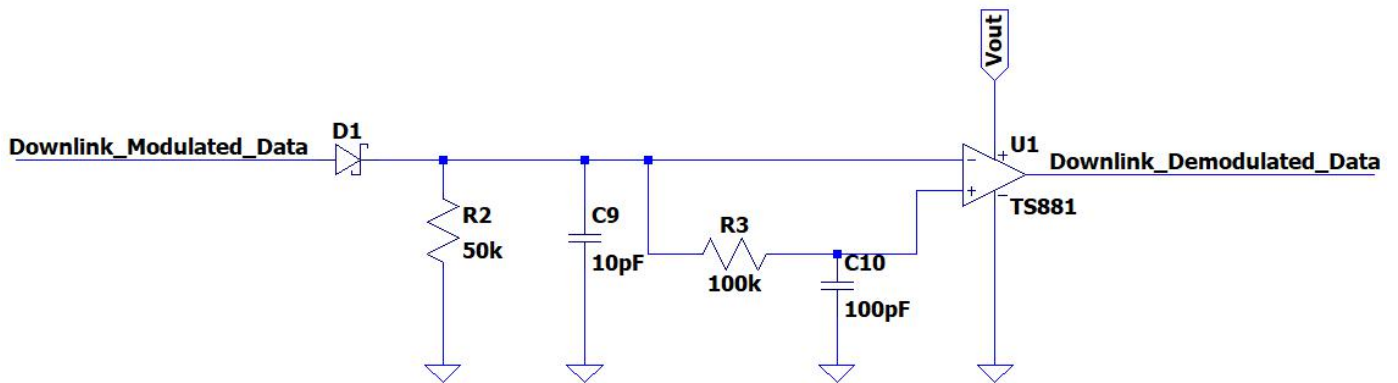


Figure 33. ASK demodulator at the receiving side

In our implementation it was chosen to have a downlink signal of around  $200kHz$ . Therefore the values of the filters' components were chosen as:  $R_2 = 50k\Omega$ ,  $C_9 = 10pF$ ,  $R_3 = 100k\Omega$ ,  $C_{10} = 100pF$ , which determine

the cut off frequencies:  $f_1 = \frac{1}{2\pi R_2 C_3} \approx 315kHz$  (28),  $f_2 = \frac{1}{2\pi R_1 C_2} \approx 16kHz$  (29).

### 4.2.4 Backscattering

Uplink communication is achieved via backscattering a.k.a. load shift keying. This is achieved by placing a transistor that operates as a switch right after the the resonating capacitor. When the switch is on, the received signal is shorted to ground and therefore the transmitting side “sees” a receiving side with a different impedance, which causes the amplitude of the transmitting sinusoidal signal to change, applying in this way an amplitude modulation in the transmitted signal. When the switch is off, it has no effect on the circuit operation. The complete receiver implementation, apart from the demodulator, is depicted in Figure 34. The switching transistor is the transistor named “*LSK\_Switch*”. Power supply “*Uplink\_Data\_10kHz*” simulates the data generated by the ZPD module.

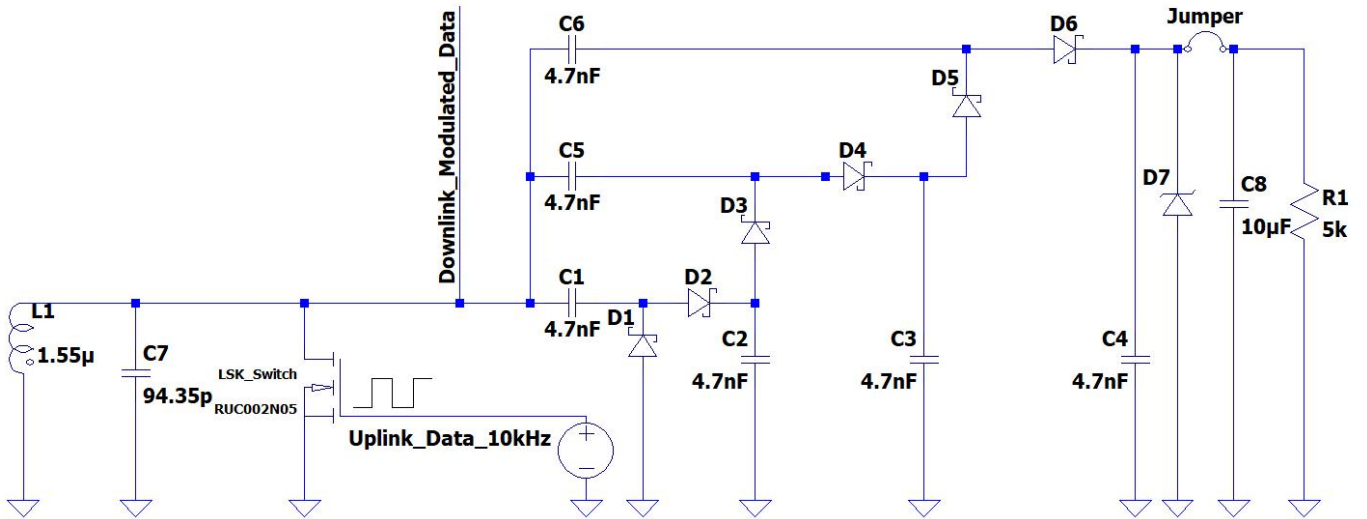


Figure 34. Receiver with backscattering

This concludes the description of the receiver. The following chapter will focus on the selection of the components, the reasoning behind it, and the manufacturing of the prototype.

# 5 Prototype Design

## 5.1 Introduction

In order to test our hypothesis, that it is possible to create a ZPD module that can be attached to the IMDs, we have decided to design and manufacture a prototype circuit using printed circuit boards (PCB). We chose to make use of the 13.56MHz for the power transfer, since it is one of the designated industrial, scientific and medical (ISM) bands and therefore built our prototype transmitter and receiver around that choice.

It was decided to almost exclusively make use of surface mounted devices (SMD), namely electronic devices and components that are placed or mounted onto the surface of the PCB, in order to reduce the size of the constructed board.

## 5.2 Component Selection

The only components that were taken for granted were the transmitting and receiving coils, as introduced before. The rest of the components were purchased from three different electronics stores: Conrad Electronics<sup>xi</sup>, Farnell Electronics<sup>xii</sup> and Mouser Electronics<sup>xiii</sup>. The components were selected with the criterion that their models were available in LTSPICE in order to have the best possible matching between the simulation results and the actual implementation. The selected components are presented in the following tables that group them according to their type. After each table the justification for the selection of these components is provided.

Table 4. Selected transistors

| Transistors      |                            |
|------------------|----------------------------|
| Name             | Value/Remarks              |
| RUC002N05HZGT116 | Fast switching MOSFET      |
| DXT3150-13       | BJT for modulation circuit |
| IRLML2030TRPBF   | Power MOSFET               |

RUC002N05HZGT116 was chosen because of its fast switching capability thanks to its low capacitance and its low  $R_{DS(on)}$  resistance that provides minimal losses when the switching occurs. It is also used to implement the buffer circuit at the demodulation circuit of the transmitting side, since in addition to its speed, it also has high input impedance and low output impedance.

DXT3150 is a transistor used for medium power switching that can provide up to 1.0W of power. Its base-emitter voltage  $V_{BE}$  of around 1.2V is relatively high, meaning it will have large power dissipation.

Finally, IRLML2030TRPBF offers fast switching capability, low  $R_{DS(on)}$  and is able to provide up to 1.3W

<sup>xi</sup> <https://www.conrad.nl/>

<sup>xii</sup> <https://www.farnell.com/>

<sup>xiii</sup> <https://nl.mouser.com/>

Table 5. Selected capacitors

| Capacitors          |                         |
|---------------------|-------------------------|
| Name                | Value/Remarks           |
| 06031A101JAT2A      | 100pF/100V              |
| MC0603N100J500CT    | 10pF/50V                |
| 06031C102JAT2A      | 1nF/100V                |
| C2012X6S1A106K085AC | 10uF/10V                |
| 12061A820JAT2A      | 82pF/10V                |
| 12065A472JAT2A      | 4.7nF/100V              |
| C0603C560G1GACTU    | 56pF/100V               |
| TZB4Z250            | 25pF trimming capacitor |
| C0603C152J5GACTU    | 1.5nF/50V               |

As far as the capacitors are concerned, all of them except for the variable ones are ceramic capacitors and therefore occupy minimal space and have low parasitic resistance and inductance. They were also chosen to adhere to the expected voltage. However, in all cases but one, the 10 $\mu$ F storage capacitor C2012X6S1A106K085A, higher voltage ratings were chosen because of the unavailability of lower rated components in the aforementioned online stores.

The 25pF trimming capacitor is used in parallel to the 82pF and 100pF capacitors in order to tune the transmitting and receiving coil.

The 10 $\mu$ F is used as a charge storage capacitor.

The 100pF, 1nF and 10pF capacitors are used in the LPFs of the demodulation circuits.

The 4.7nF capacitors are used in the implementation of the 3 stage charge pump rectifier.

The 56pF capacitor is used in the class-E amplifier circuit.

The 1.5nF capacitor is used at the capacitive divider

Table 6. Selected diodes

| Diodes         |                             |
|----------------|-----------------------------|
| Name           | Value/Remarks               |
| CDZFHT2RA6.2B  | Zener Diode                 |
| MBR0520L       | Schottky Rectifier Diodes   |
| RB751G-40FHT2R | Small signal Schottky Diode |

The zener diode CDZFHT2RA6.2B is used as an overvoltage protection measure. Its 6.2V reverse voltage  $V_r$  does not provide good protection for most of the modern systems that operate in the region between

3.3V and 5.0V. A Zener diode with a reverse voltage of 5V would be a better choice, but it was chosen for the sake of acquiring more measurements.

The rectifier diode MBR0520L is ideal for switching since it offers a forward voltage  $V_F$  of around 300mV. 6 diodes of this type are used to implement the 3 stage charge pump rectifier.

The small signal diode RB751G-40FHT2R also offers a low forward voltage  $V_F$  of around 350mV and is used at the envelope detectors of both demodulation circuits.

Table 7. Selected resistors

| Resistors        |               |
|------------------|---------------|
| Name             | Value/Remarks |
| MCWR06X4992FTL   | 50k $\Omega$  |
| RC0603FR-13100KL | 100k $\Omega$ |
| ERJ3GEYJ165V     | 1.6M          |
| MCWR06W3304FTL   | 3.3M          |
| 3224W-1-103E     | 10k trimmer   |

The 100k resistor is used at the buffer circuit.

The 100k, 50k 1.6M and 3.3M resistors are used in the envelope detectors and LPFs of the demodulation circuits.

The 10k trimmers are used in the ASK modulation circuit to define the modulation index. One trimmer could have been enough to set the modulation index, but we chose to have two trimmer resistors in order to have better control over it.

Table 8. Selected inductors

| Inductors    |                |
|--------------|----------------|
| Name         | Value/Remarks  |
| RLB0913-3R3K | 3.3uH inductor |
| 744773014    | 1.4uH inductor |

The 3.3uH and 1.4uH inductors are used in the class-E amplifier as an RF choke and tuning inductor respectively. They have low series resistances and sufficient margins as far as the rated current is concerned. It has to be noted that the 3.3uH inductor is the only through hole electrical component used in our implementation.

Table 9. Selected comparator

| Comparator |                      |
|------------|----------------------|
| Name       | Value/Remarks        |
| TS881ILT   | Nanopower comparator |

The TS881ILT comparator is used in both demodulation circuits. It requires only a minimal supply current of 300nA. Its maximum voltage limit of 6.0V is the reason why a capacitive divider has to be used at the output of the transmitting circuit in order to achieve the demodulation of the uplink signal.

### 5.3 PCB Design and Assembly

Two separate PCBs were designed; one for the transmitting and one for the receiving side. The software used for designing the PCBs was Autodesk EAGLE. Both PCBs were basic implementations of 2 layers. Since the coils used as transceivers occupy a lot of space, are heavy and are printed on separate PCBs, they are connected to the circuit via an SMA port. Both the transmitter and the receiver were over-designed as far as size is concerned, so that also mechanical stability could be guaranteed. Figures 35 and 36 depict the designs of the transmitter and receiver PCBs, respectively.

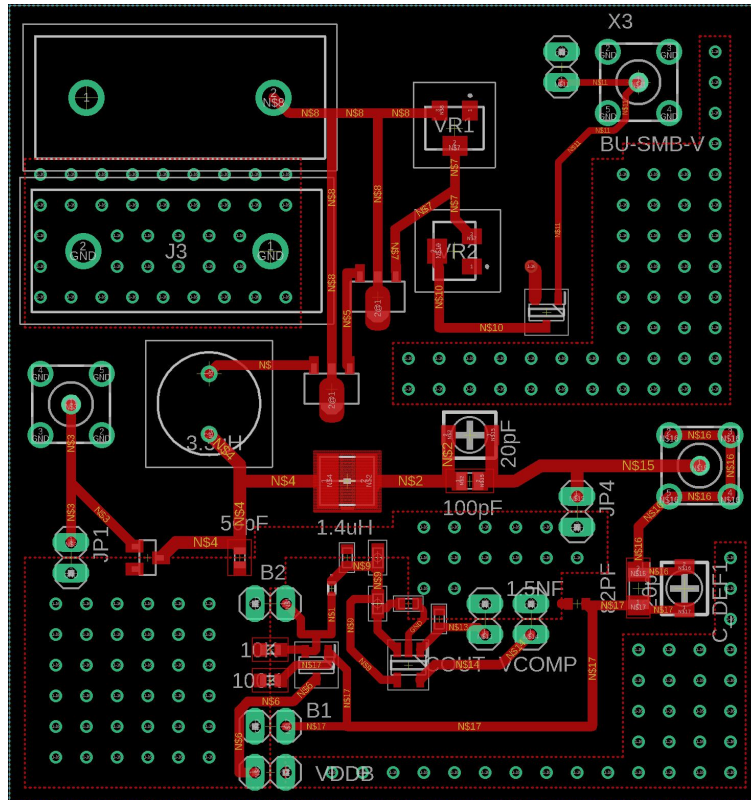


Figure 35. PCB design of the transmitter

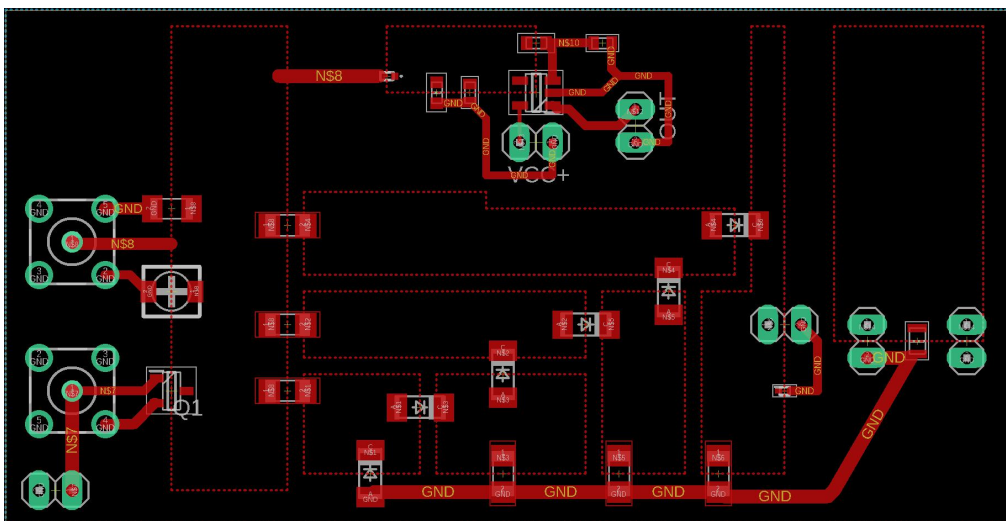


Figure 36. PCB design of the receiver

Both PCBs were designed to have their whole bottom side as ground plane. It is noteworthy that in the transmitter side many via nodes were used in order to help dissipate the expected heat created by the power transistors in the ground plane more effectively. One can also observe that, in the receiver, the storage capacitor is not directly connected to the output of the rectifier. Instead of connecting it directly, two junction points were placed that can be connected externally with a cable. The reason behind this is that we wanted to have the possibility to connect a power management IC between these two junctions that would regulate the power provided by the rectifier to the capacitor and from the capacitor to the load.

The internet databases of Samacsys<sup>xiv</sup>, Octopart<sup>xv</sup> and Ultralibrarian<sup>xvi</sup> were used to acquire the exact PCB traces of the selected components. After finishing the design, the Gerber files were extracted and sent for assembly. When the PCBs arrived, all the components were soldered giving the final results can be seen in Figures 37 and 38.



Figure 37. Transmitter PCB

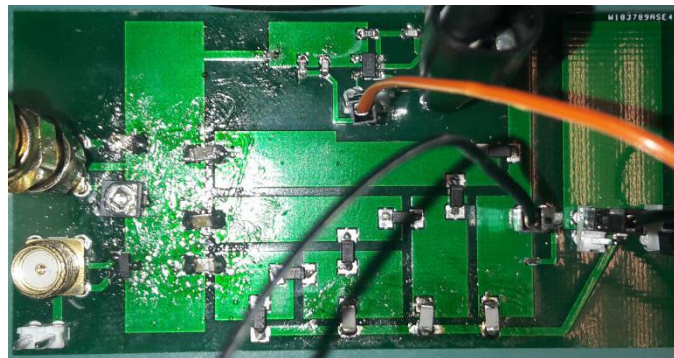


Figure 38. Receiver PCB

With both the transmitter and receiver fully assembled we then proceeded to the measurement and characterization of the link, which constitutes the following chapter.

<sup>xiv</sup> <https://www.samacsys.com/>

<sup>xv</sup> <https://octopart.com/>

<sup>xvi</sup> <https://www.ultralibrarian.com/>

# 6 Measurements and Characterization of the Link

## 6.1 Measurement Setup and Additional Equipment

The measurement setup is depicted in Figure 39.

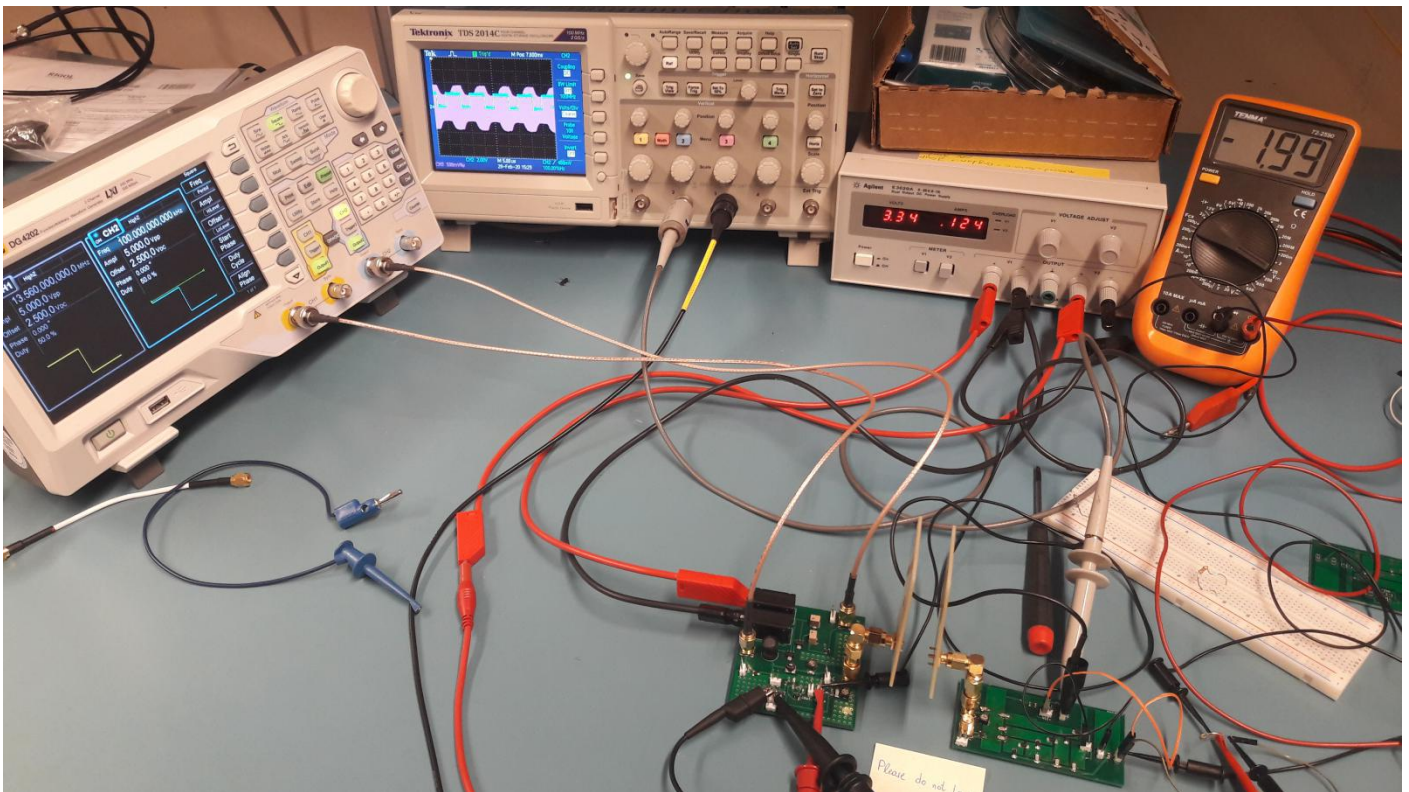


Figure 39. Complete measurement setup

One can observe in Figure 39, that apart from the PCBs and the antennas, a digital oscilloscope, a Waveform Generator, a DC power supply as well as two multimeters were used. The depicted equipment is listed in Table 10.

Table 10. Additional lab equipment

| Equipment type     | Model                        |
|--------------------|------------------------------|
| Oscilloscope       | Tektronix TDS 2014C          |
| Waveform Generator | Rigol DG4202                 |
| Power Supply       | Agilent E3620A               |
| Multimeters        | Tenma 72-7732, Tenma 72-2590 |

## 6.2 Limitations

The measurements contain a number of limitations that have to be mentioned.

First of all, in the electronics lab, there are many signals from the various devices and laboratory equipment that can interfere with the measured signals of our prototype. This, in addition to the use of probes with elongated cables makes it easier to pick up interfering signals from the environment. Also, in a real life scenario the receiving circuit, except for the antenna, would be shielded and therefore would not pick up any signal from the transmitter, which is not the case in this prototype that is exposed to radiation. It has to be noted here that in a real-life scenario, the receiver would have a much smaller form factor. Therefore, the only source of interference is going to be the receiving antenna.

Moreover, it was decided to move the antennas freely, without constraining their movement with designated barriers that would make sure that the coils would always have the best possible alignment. This was done in order to simulate possible coil misalignment between the transmitting and the receiving antennas, a phenomenon that is frequent in this type of communication.

## 6.3 Measurements

### 6.3.1 Receiver Detuning

First of all, it has to be noted that the trade-off of detuning the receiver in order to fit a three stage charge pump rectifier that was taken during the design phase, could be justified by changing the value of the trimmer capacitor that was placed in parallel to the receiving antenna to help tune it to resonance. This change in capacitance had no effect in the transmitted power, which means that the equivalent capacitance “seen” by the receiving antenna in parallel is probably orders of magnitude higher than the capacitance meant to resonate the antenna, which was around 100pF.

### 6.3.2 Wireless Power Transfer

The first parameter that was tested was tested was the ability of the circuit to transfer power to the receiver circuit. The measurements that were taken were conducted in the following way. The DC output voltage of the load was monitored with the use of a multimeter and a probe. Power was provided to the transmitting side by the DC power supply. That voltage was set a specific level (3, 4, 5, 6 volts) and then measurements of the output voltage were taken after varying the distance of the transmitting and receiving antennas. The distance was varied between 0.9 and 3.0 centimetres. Figure 40 depicts the measured voltage as well as the demodulated signal at the receiver side.

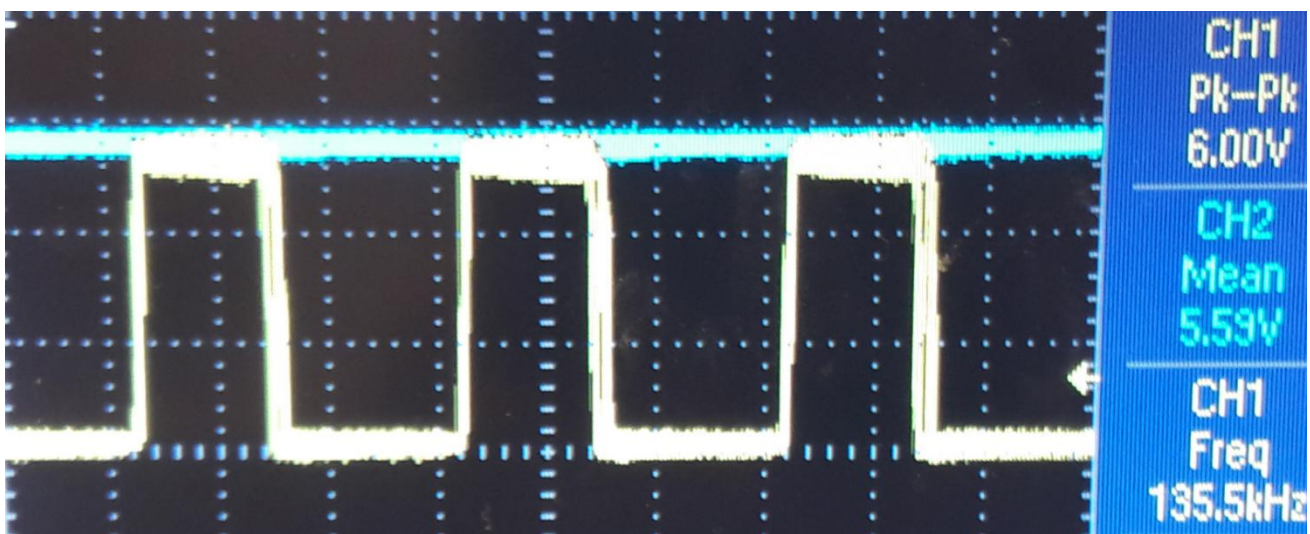


Figure 40. Output voltage and demodulated signal

Figures 41 - 44 depict graphs that accumulate the output power measurements that were obtained. In all the measurements that used modulation, the modulation frequency was 100kHz. The supply voltage was changed for every set of measurements. In each graph the power at the load of the receiver is depicted, while the supply voltage of the transmitter in the current set of measurements is mentioned at the title of each graph. In these graphs, a comparison is made between the received power that one gets when there is no amplitude modulation (blue) of the transmitted signal and the power when there is modulation (red).

When the supply voltage of the transmitter is 3V (Figure 41), the maximum power at the output of the receiver was measured to be 3.58mW with data modulation from the transmitter active and 5.17mW without any modulation. The 2.2mW goal is achievable in a distance of up to 1.2cm when data modulation is active and up to 1.5cm when data modulation is inactive.

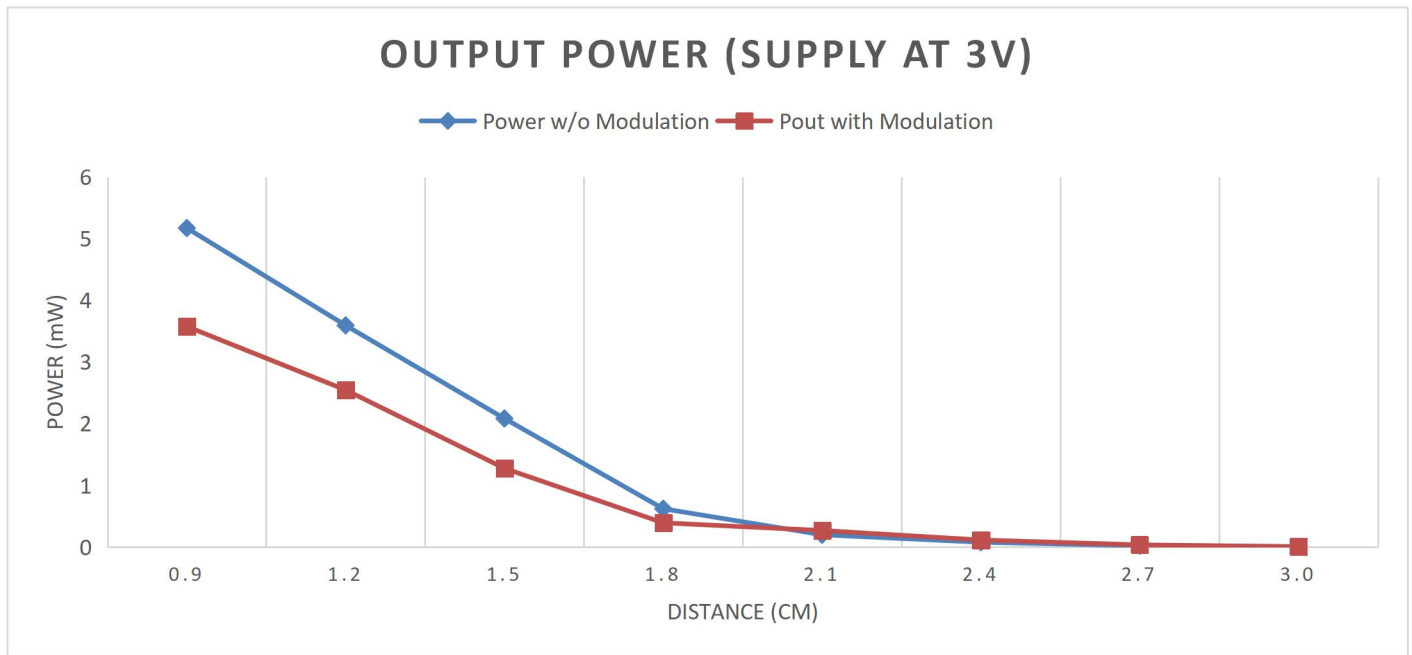


Figure 41. Output power over distance with 3V supply

When the supply voltage of the transmitter is 4V(Figure 42), the maximum power at the output of the receiver was measured to be 6.2mW with data modulation from the transmitter active and 7.66mW without any modulation. The 2.2mW goal is achievable in a distance of up to 1.5cm when data modulation is active and up to 1.8cm when data modulation is inactive.

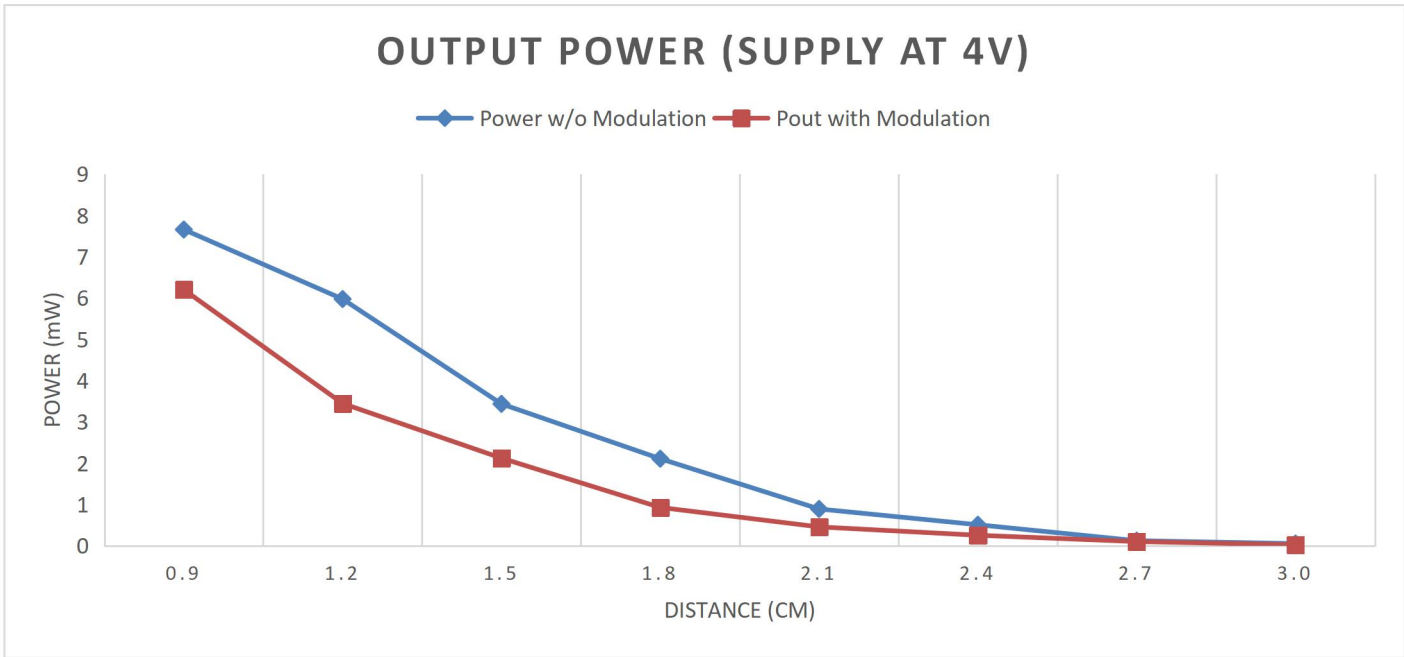


Figure 42. Output power over distance with 4V supply

When the supply voltage of the transmitter is 5V, the maximum power at the output of the receiver was measured to be 7.66mW with data modulation from the transmitter active and 7.66mW without any modulation, which is the maximum achievable value due to the use of the overvoltage protection diode. The 2.2mW goal is achievable in a distance of up to 2.1cm both when data modulation is active and when it is inactive.

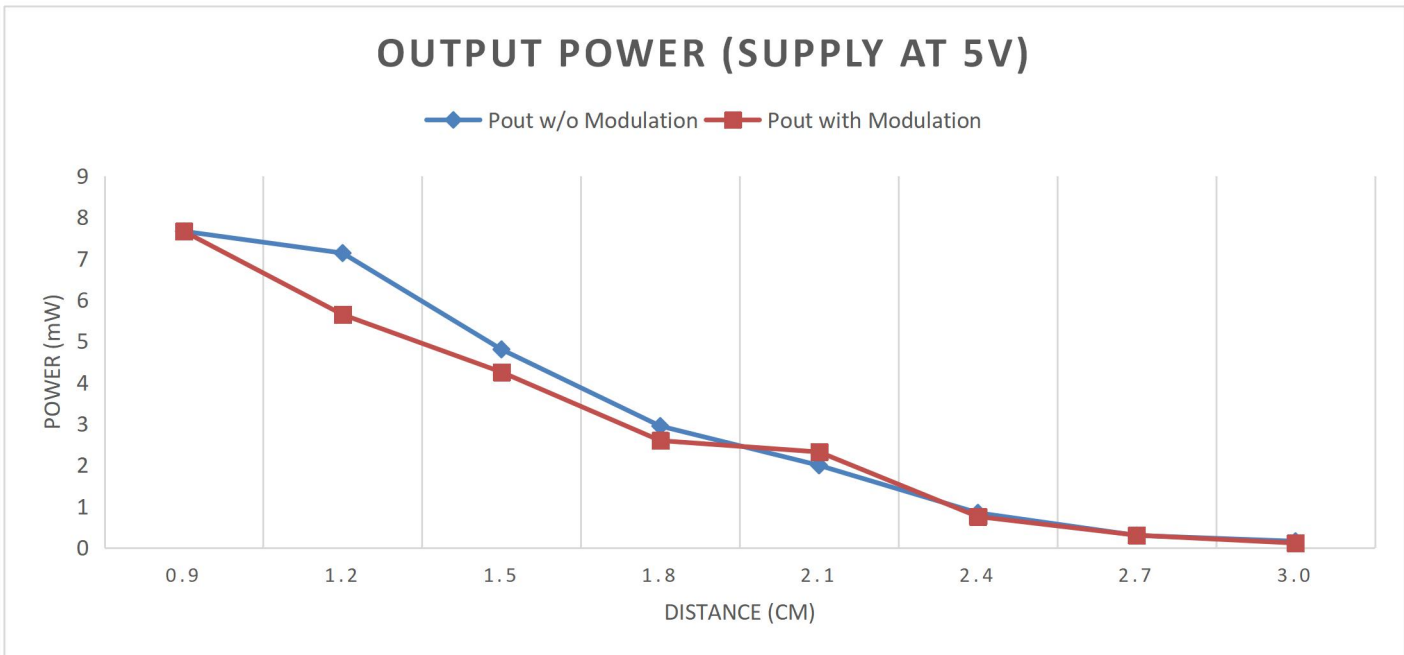


Figure 43. Output power over distance with 5V supply

When the supply voltage of the transmitter is 6V, the maximum power at the output of the receiver was measured to be 7.66mW with data modulation from the transmitter active and 7.66mW without any modulation, which is the maximum achievable value due to the use of the overvoltage protection diode. The 2.2mW goal is achievable in a distance of up to 2.1cm both when data modulation is active and when it is inactive.

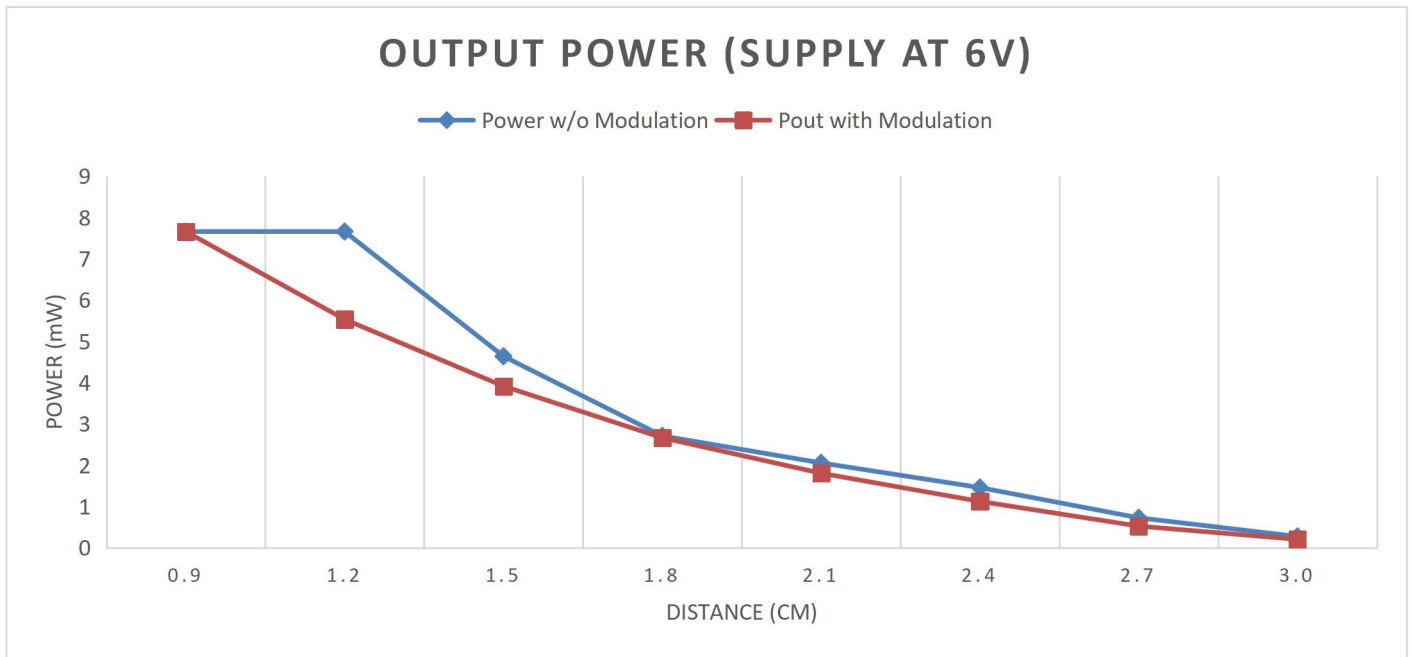


Figure 44. Output power over Distance with 6V supply

From these Figures one can observe that the received power drops almost hyperbolically with the increase of the distance, which is in line with the theory. Moreover, one can also distinguish the reduced amount of power when amplitude modulation is on.

Since the required power levels were around 2.0 milliwatts, the prototype is successful at delivering sufficient amounts of power at a maximum distance of around 2.0 centimetres. Finally, it is notable that the maximum power delivered to the load is limited by the zener diode that does not allow the power delivered to the load exceed 7.66 milliwatts.

### 6.3.2 Maximum Detectable Frequency

Before presenting the results of the measurements, we should first clarify what detectable frequency means. It means, that the measured demodulated signal had a duty cycle close to 50% as depicted in Figure 45, where the modulated transmitted signal as well as the demodulated signal at the receiver are depicted.

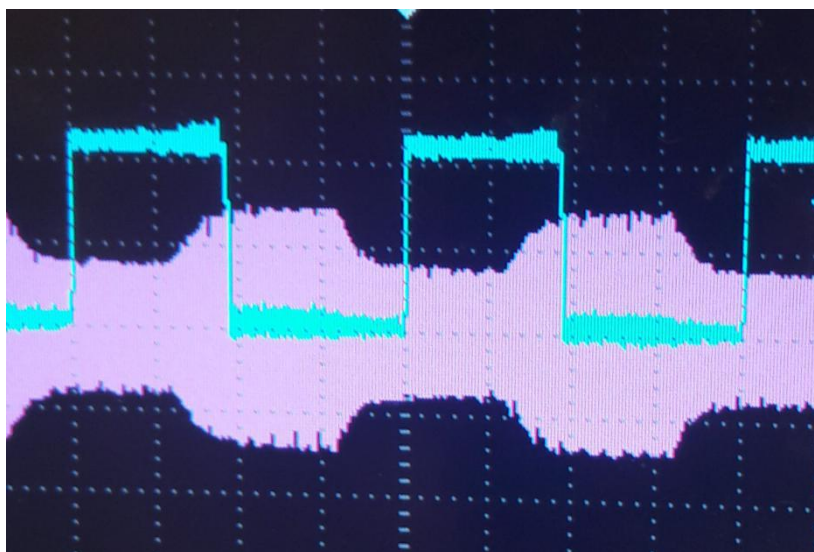


Figure 45. Received downlink modulated signal (pink) and demodulated signal (teal)

For this measurement the supply voltage was set at a certain value and the receiver antenna was placed at designated distances from the transmitter. Then the frequency of the transmitted signal was increased until the demodulated signal became undetectable because either the jitter became too high or the signal's duty cycle became more than around 60%. The results are summed up in Figure 46 that depicts a graph of the measurements taken.

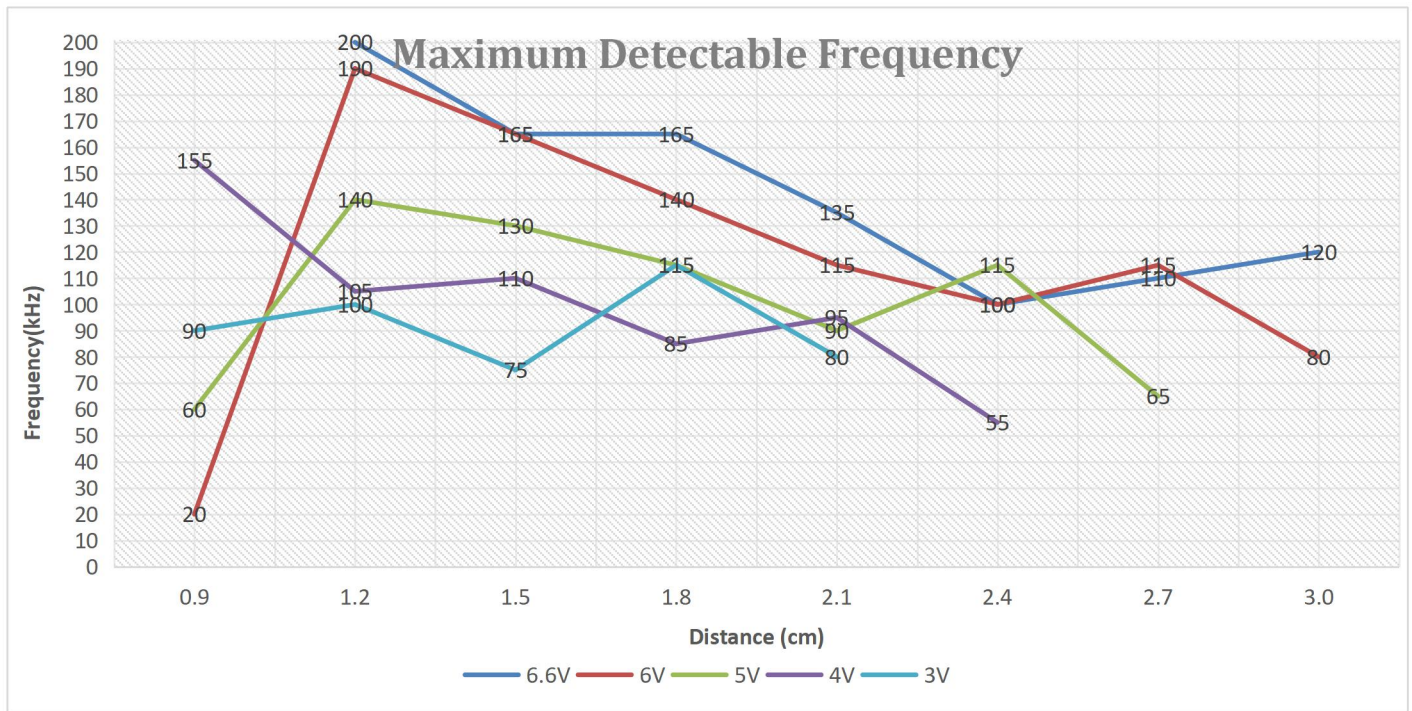


Figure 46. Maximum detectable modulation frequencies over distance

The maximum modulation frequency that could be reliably detected was 200 kHz at a distance of 1.2cm when the voltage fed into the transmitter from the power supply was 6.6V. It can be observed that the higher the voltage fed to the transmitter is, the higher the achievable modulation frequencies are. However, with higher voltage fed to the transmitter, the received signal has higher voltage ripple. The distance of 1.2 cm seems to be the distance where the highest frequencies are achieved, except the case where the voltage fed to the transmitter is 3V. In this case the maximum achieved frequency was 115kHz at a distance of 1.8cm.

It is noteworthy that the modulation index plays an important role in the demodulated received signal. The increase of the modulation rate causes jitter as can be seen from Figures 47 and 48 where the modulation index is 22.9% and 36.6% in comparison with Figure 40 that has a modulation index of 50%.

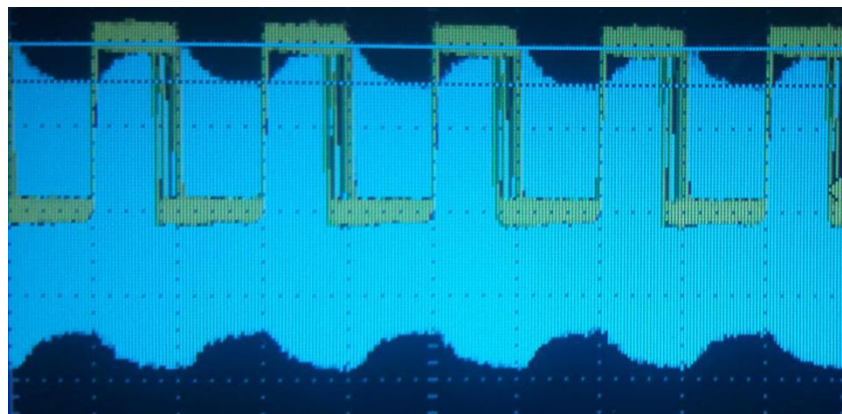


Figure 47. Transmitted signal (teal) and demodulated data (yellow) with MI = 22.9%

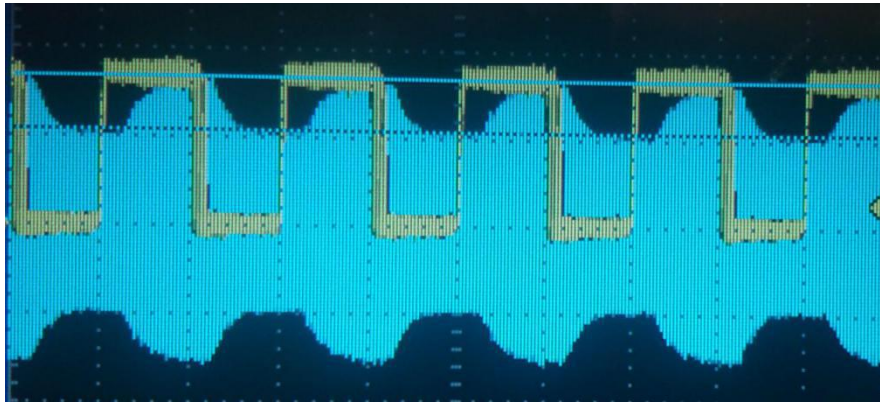


Figure 48. Transmitted signal (teal) and demodulated data (yellow) with MI = 36.6%

Taking everything into account, the designed prototype is able to transmit power and downlink data reliably in low distances. Providing higher input power increases the amount of power transmitted, but also reduces the power transfer efficiency of the system, as can be seen by the measurements in the appendix. Also, with increased transmitted power, higher frequencies were able to be demodulated, but the ripple of the output was simultaneously increased. However, the output voltage of the rectifier is used to also provide the  $V_{cc}$  of the comparator. This means that the ripple caused in the output is also going to exist in the output of the rectifier. This in turn introduced ripple in the demodulated waveform.

## 6.4 Backscattering

As far as the uplink is concerned, the effect of backscattering (a.k.a. LSK) can be observed in Figure 49, that depicts the transmitted signal when the LSK is taking place, as well as the demodulated signal at the transmitter side. The frequency used in this measurement was 2kHz. The voltage difference observed at the transmitted signal is 100mV, which makes it detectable by our demodulation circuit.

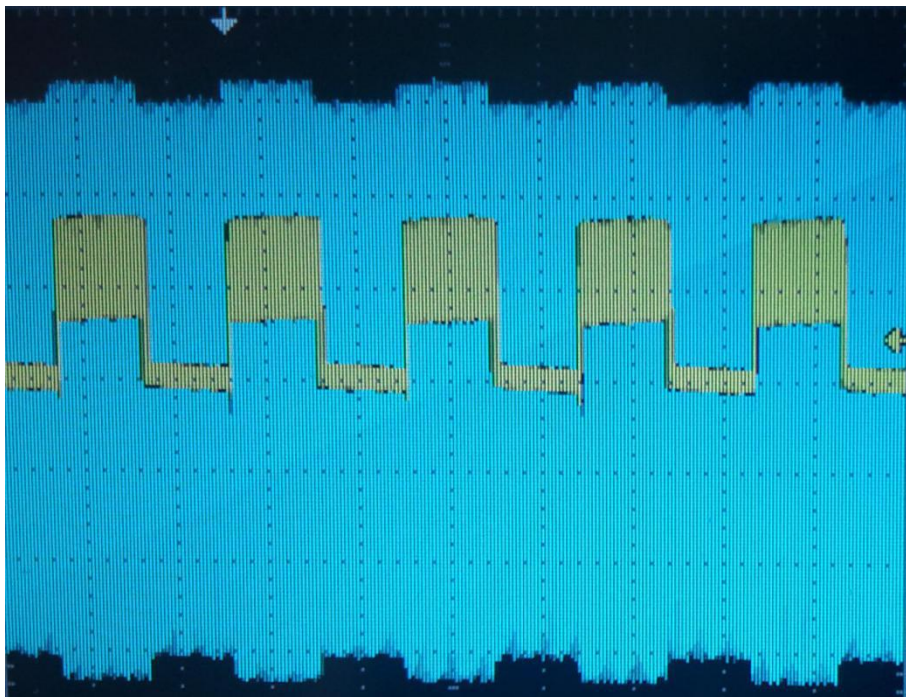


Figure 49. Transmitted signal (teal) during backscattering and demodulated uplink signal (yellow)

One can easily observe an interference on the retrieved signal. This interference was a 6.86MHz, 1Vp-p sinusoid. Moreover, when the frequency of the LSK was increased, the relative jitter also increased. Several

measurements were taken, but it was observed that the backscattered signal could only be detected when a specific set of conditions was met:

- The antennas were placed at the specific distance of 0.9 cm
- The supply voltage was at 2.48V
- The comparator voltage was at 1.16V

Under these conditions the voltage at the output of the receiver was measured to be 3.24V, which means that the power requirements were marginally met. If these conditions are not met the backscattered signal was not detectable.

The highest detectable frequency of the backscattered pulses was around 1kHz. During the experimentation, it was observed that lowering the duty cycle of the pulses led to an increase of the frequency that was detectable. More specifically, at 20% duty cycle the maximum detected frequency in the received signals was 10kHz. However these measurements were not taken into account, since only signals between 40% and 60% duty cycle were considered as acceptable, as was the case in subsection 6.3.2.

This behaviour comes in contrast with the simulations that were taken during the design process of the circuit. In Figure 50 one can observe that the backscattered signal is easily detectable from the transmitting side of the system. This can be explained by the fact that in simulations neither electromagnetic interference sources nor the tolerances of the various components were taken into account. Moreover, the simulation software does not take into account the distance between the transmitting and receiving antennas and their misalignment.

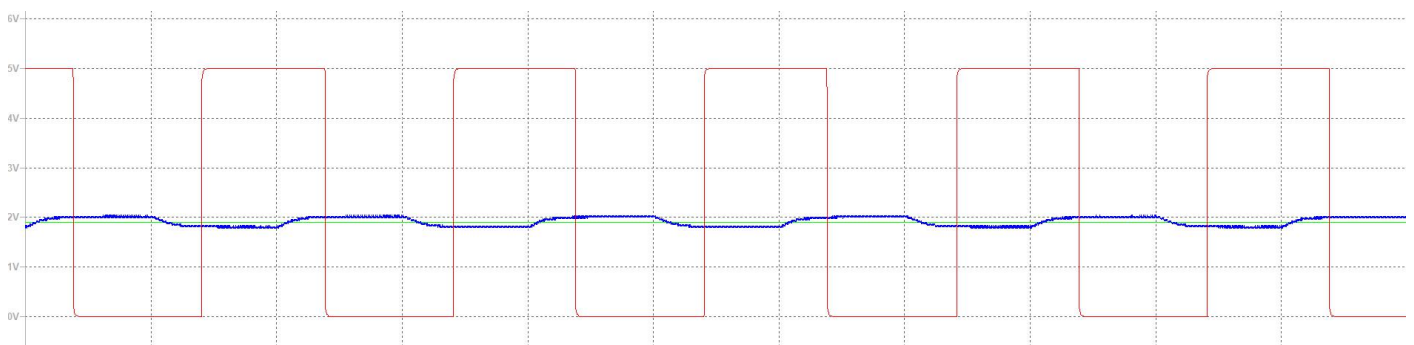


Figure 50. Simulation waveforms of backscattered a) envelope detected signal (blue), b) averaged (green) and c) demodulated signal (red)

## 6.5 Result Summary

Taking everything into account, the designed prototype proved successful in transferring power and data over small distances. The 2.2mW and a voltage of more than 3V at the output was achieved both for modulated and non-modulated signals at maximum distances of 1.5cm and 1.8cm respectively.

The maximum frequency of the transmitted signal varies depending on the distance between the antennas as well as the DC voltage and therefore the power that is provided by the supply of the transmitter. The maximum achieved frequency was 200kHz at a distance of 1.2cm. The maximum modulation index where the demodulated signal had acceptable duty cycle and jitter was 35%.

As far as the backscattered signal is concerned, the designed link proved to be unreliable and only able to work under certain circumstances, meaning that there is one 'sweet spot' where the coupling is best and so the change of impedance at the receiver due to LSK creates a measurable voltage change at the transmitter. This can be explained by the fact that the receiver is detuned from resonance because of the large capacitance required for the charge pump rectifier compared to the one required to resonate the receiving antenna and therefore the receiver is not seen as a purely ohmic load by the transmitter.

It is also worth noting, that measurements were taken with human tissue, namely the hand of the experimenter, between the antennas. This interference of tissue between the antennas had no effect in the transfer of power and data to the receiver, as it was expected since the human tissue is nearly transparent to radiation at 13.56MHz. Moreover, no heating of any of the receiver elements was observed.

# 7 Conclusions

## 7.1 Contributions

In this thesis, an experimental prototype for power and data transmission has been designed and implemented. The design was based on the idea of Zero Power Defence and was meant to simulate a module that can receive power and data from a reader outside of the human body and can transmit data back to that reader in order to decide whether the person trying to communicate with the IMD is authorized to do so by executing a handshake between them.

This prototype was successful in transferring enough power according to the given specifications of 2.2mW, while also exceeding the required 3V for a substantial range of distances. The data was modulated using ASK for the downlink and LSK for the uplink communication. The downlink proved reliable and able to work up to 3.0cm distance between the antennas, achieving a maximum data rate of 200kbit/s at a distance of 1.2cm. The uplink communication channel was unstable and not dependable, since we could only make it operational under certain circumstances. This can be explained by the weak coupling between the coils, the detuning of the receiver circuit by the added capacitances of the components comprising the rectifier and demodulator circuits, as was mentioned earlier in Section 6.4, the possible inaccuracies of the components in the demodulation circuit of the transmitter as well as by the effect of EMI from the antennas and the laboratory equipment. Taking the aforementioned in consideration, this prototype could be used for a ZPD scheme aimed to counter the BDoS attacks.

## 7.2 Discussion

As far as published literature is concerned, the work of this thesis is being compared to published papers in Table 11.

Table 11. Comparison table

| Work      | Power Transferred (mW) | Power fed to the Transmitter (mW) | Rectifier Output Voltage (V) | Operating Frequency (MHz) | Downlink Modulation Rate <sup>xvii</sup> (%) | Downlink Modulation Index (%) | Downlink Data Rate (bits/s) | Uplink Data Rate (bits/s) |
|-----------|------------------------|-----------------------------------|------------------------------|---------------------------|--|-------------------------------|-----------------------------|---------------------------|
| [53]      | 165                    | 250                               | 6                            | 13.56                     | 7.3  | 13                            | 10 <sup>6</sup>             | -                         |
| [54]      | 136.6                  | 274                               | -                            | 13.56                     | 18.25  | 11                            | 10 <sup>6</sup>             | -                         |
| [55]      | 165                    | 250                               | 3.0                          | 13.56                     | 0.73   | 12.6                          | 10 <sup>5</sup>             | -                         |
| [31]      | -                      | -                                 | -                            | 2                         | 50   | 5.26                          | 10 <sup>6</sup>             | -                         |
| [33]      | -                      | -                                 | -                            | 2                         | 50   | 2.86                          | 10 <sup>6</sup>             | -                         |
| [56]      | -                      | -                                 | -                            | 2                         | 28.5   | 10                            | 5.7*10 <sup>5</sup>         | -                         |
| [10]      | 102                    | -                                 | 3.6                          | 13.56                     | -  | -                             | -                           | 3*10 <sup>4</sup>         |
| [19]      | 11.2                   | 1100                              | 3.6                          | 13.56                     | -  | -                             | -                           | 600                       |
| This work | 8 <sup>xviii</sup>     | 2600                              | 6.1                          | 13.56                     | 1.46   | 35                            | 2*10 <sup>5</sup>           | 10 <sup>3</sup>           |

$$^{xvii} \text{ Modulation Rate} = \frac{\text{Data Rate}}{\text{Operating Frequency}} * 100\%$$

<sup>xviii</sup> Transferred power in our work was measured at the load, while in the other works it was measured at the receiving antenna

Before the comparison is made, it must be noted that [31], [33] and [56] were focused only on designing the ASK demodulator of an IMD without paying any attention to wireless power transfer, while [10], [19] did not implement any downlink data link.

Compared to the other works, our implementation is lacking in the amount of power transmitted to the receiver. However, [53], [54], [55], [10] and [19] were designed to provide power for the complete operation of IMDs and not for the operation of just one small module meant to act as an add-on to the IMD. Moreover, a decent downlink data rate with a maximum of 200kbit/s was achieved. This value is higher than the 100kbit/s that were achieved in [63], but lower than the other works that implemented data transfer from the reader to the IMD.

The uplink was able to operate only under certain conditions and reached a mere data rate of 1kbit/s instead of the designed 20kbit/s, the reasons being mentioned above. This value is higher than the 600bit/s achieved by [19] but much lower than the 30kbit/s achieved by [10].

Our work is the only one of the compared papers that implemented a completely independent, wirelessly-powered module with a highly asymmetrical data link between it and an external reader, by making use of ASK and LSK. This makes the designed system suitable for the task of establishing secure communication between the two entities with exchange of information between them, provided that some improvements are made. Namely, a better implementation of the uplink would make the system much more robust and more suitable for the task. The use of discrete components, whose values have certain tolerances, the exposure of the system in EMI without any shielding and the use of high capacitance for the charge pump rectifier that results in loss of resonance between the antennas contribute to the reduced operation of the backscattering link and the total amount of power transferred. However, it should always be kept in mind that this design was based on proving functionality and not optimization of performance. Some recommendations to improve the overall performance are made in Section 7.3.

### 7.3 Recommendations for future work

Although satisfying wireless power and data transfer were achieved by the proof-of-concept prototype designed for this thesis, there are some aspects of the originally designed system that were not examined. Only the wireless power transfer has been successfully tested with a micro-controller. It would therefore be beneficial to use micro-controllers both in the reader and in the module side in order to generate and read the data. In this way we would also be able to test the bit error rate (BER) of the designed prototype. Moreover, if the system was to be redesigned, more attention should be given to the implementation of the receiving side in order to achieve better resonance that will also improve the operation of the backscattering. Furthermore, the whole system could be redesigned on an ASIC that will include all the parts of the module. In this way its size as well as power consumption will be minimized. Moreover, the whole concept of this thesis could be implemented for longer distance scenarios by making use of a different Wireless Power Transfer method, or Energy Harvesting methods optimized for longer distances. Such a case would be the scenario of having a bedside monitor that exchanges data with an IMD inside a patient that is sleeping in the bed in the proximity of the monitor. Finally, it would also be beneficial to conduct SAR measurements using accurate models of the human body, in order to further test the effect of the radiation absorbed by the human tissue.

# Bibliography

- 1 Agarwal, K., Jegadeesan, R., Guo, Y.-X., and Thakor, N.V.: 'Wireless power transfer strategies for implantable bioelectronics', *IEEE Reviews in Biomedical Engineering*, 2017, 10, pp. 136-161
- 2 Bashirullah, R.: 'Wireless implants', *IEEE microwave magazine*, 2010, 11, (7), pp. S14-S23
- 3 Serdijn, W., Mansano, A., and Stoopman, M.: 'Introduction to RF energy harvesting': 'Wearable Sensors' (Elsevier, 2014), pp. 299-322
- 4 Siddiqi, M.A., and Strydis, C.: 'Towards realistic battery-DoS protection of implantable medical devices', in Editor (Ed.)^(Eds.): 'Book Towards realistic battery-DoS protection of implantable medical devices' (2019, edn.), pp. 42-49
- 5 Belkhouja, T., Mohamed, A., Al-Ali, A.K., Du, X., and Guizani, M.: 'Light-Weight Solution to Defend Implantable Medical Devices against Man-In-The-Middle Attack', in Editor (Ed.)^(Eds.): 'Book Light-Weight Solution to Defend Implantable Medical Devices against Man-In-The-Middle Attack' (IEEE, 2018, edn.), pp. 1-5
- 6 Halperin, D., Heydt-Benjamin, T.S., Ransford, B., Clark, S.S., Defend, B., Morgan, W., Fu, K., Kohno, T., and Maisel, W.H.: 'Pacemakers and implantable cardiac defibrillators: Software radio attacks and zero-power defenses', in Editor (Ed.)^(Eds.): 'Book Pacemakers and implantable cardiac defibrillators: Software radio attacks and zero-power defenses' (IEEE, 2008, edn.), pp. 129-142
- 7 Ellouze, N., Allouche, M., Ben Ahmed, H., Rekhis, S., and Boudriga, N.: 'Securing implantable cardiac medical devices: Use of radio frequency energy harvesting', in Editor (Ed.)^(Eds.): 'Book Securing implantable cardiac medical devices: Use of radio frequency energy harvesting' (2013, edn.), pp. 35-42
- 8 Seepers, R.: 'Implantable Medical Devices: Device security and emergency access', 2016
- 9 Asgarian, F., Sodagar, A.M., and Laskovski, A.: 'Wireless telemetry for implantable biomedical microsystems', *Biomedical Engineering, Trends in Electronics, Communications and Software*, 2011, pp. 21-44
- 10 Li, X., Tsui, C.-Y., and Ki, W.-H.: 'A 13.56 MHz wireless power transfer system with reconfigurable resonant regulating rectifier and wireless power control for implantable medical devices', *IEEE Journal of Solid-State Circuits*, 2015, 50, (4), pp. 978-989
- 11 Balanis, C.A.: 'Antenna theory: A review', *Proceedings of the IEEE*, 1992, 80, (1), pp. 7-23
- 12 Prince, J.L., and Links, J.M.: 'Medical imaging signals and systems' (Pearson Prentice Hall Upper Saddle River, NJ, 2006. 2006)
- 13 Ahn, D., and Hong, S.: 'Wireless power transmission with self-regulated output voltage for biomedical implant', *IEEE Transactions on Industrial Electronics*, 2013, 61, (5), pp. 2225-2235
- 14 Catrysse, M., Hermans, B., and Puers, R.: 'An inductive power system with integrated bi-directional data-transmission', *Sensors and Actuators A: Physical*, 2004, 115, (2-3), pp. 221-229
- 15 Schormans, M., Valente, V., and Demosthenous, A.: 'Practical inductive link design for biomedical wireless power transfer: A tutorial', *IEEE transactions on biomedical circuits and systems*, 2018, 12, (5), pp. 1112-1130
- 16 Wang, G., Wang, P., Tang, Y., and Liu, W.: 'Analysis of dual band power and data telemetry for biomedical implants', *IEEE Transactions on biomedical circuits and systems*, 2011, 6, (3), pp. 208-215
- 17 Bihl, U., Liu, T., and Ortmanns, M.: 'Telemetry for implantable medical devices: Part 3-Data telemetry', *IEEE Solid-State Circuits Magazine*, 2014, 6, (4), pp. 56-62
- 18 Lee, B., and Ghovanloo, M.: 'An overview of data telemetry in inductively powered implantable biomedical devices', *IEEE Communications Magazine*, 2019, 57, (2), pp. 74-80
- 19 Kiani, M., and Ghovanloo, M.: 'A closed loop wireless power transmission system using a commercial RFID transceiver for biomedical applications', in Editor (Ed.)^(Eds.): 'Book A closed loop wireless power transmission system using a commercial RFID transceiver for biomedical applications' (IEEE, 2009, edn.), pp. 3841-3844
- 20 Jiang, D., Cirmirakis, D., Schormans, M., Perkins, T.A., Donaldson, N., and Demosthenous, A.: 'An integrated passive phase-shift keying modulator for biomedical implants with power telemetry over a single inductive link', *IEEE transactions on biomedical circuits and systems*, 2016, 11, (1), pp. 64-77
- 21 Mirbozorgi, S.A., Yeon, P., and Ghovanloo, M.: 'Robust wireless power transmission to mm-sized free-floating distributed implants', *IEEE transactions on biomedical circuits and systems*, 2017, 11, (3), pp. 692-702
- 22 Jegadeesan, R., Agarwal, K., Guo, Y.-X., Yen, S.-C., and Thakor, N.V.: 'Wireless power delivery to flexible subcutaneous implants using capacitive coupling', *IEEE Transactions on Microwave Theory and Techniques*, 2016, 65, (1), pp. 280-292
- 23 Ozeri, S., and Shmilovitz, D.: 'Ultrasonic transcutaneous energy transfer for powering implanted devices', *Ultrasonics*, 2010, 50, (6), pp. 556-566
- 24 Charthad, J., Weber, M.J., Chang, T.C., and Arbabian, A.: 'A mm-sized implantable medical device (IMD) with ultrasonic power transfer and a hybrid bi-directional data link', *IEEE Journal of solid-state circuits*, 2015, 50, (8), pp. 1741-1753

- 25 Ozeri, S., and Shmilovitz, D.: 'Simultaneous backward data transmission and power harvesting in an ultrasonic transcutaneous energy transfer link employing acoustically dependent electric impedance modulation', *Ultrasonics*, 2014, 54, (7), pp. 1929-1937
- 26 Shmilovitz, D., Ozeri, S., Wang, C.-C., and Spivak, B.: 'Noninvasive control of the power transferred to an implanted device by an ultrasonic transcutaneous energy transfer link', *IEEE Transactions on Biomedical Engineering*, 2013, 61, (4), pp. 995-1004
- 27 Costanzo, A., and Masotti, D.: 'Smart solutions in smart spaces: Getting the most from far-field wireless power transfer', *IEEE Microwave Magazine*, 2016, 17, (5), pp. 30-45
- 28 Liu, C., Guo, Y.-X., Sun, H., and Xiao, S.: 'Design and safety considerations of an implantable rectenna for far-field wireless power transfer', *IEEE Transactions on antennas and Propagation*, 2014, 62, (11), pp. 5798-5806
- 29 Sawan, M., Hu, Y., and Coulombe, J.: 'Wireless smart implants dedicated to multichannel monitoring and microstimulation', *IEEE Circuits and systems magazine*, 2005, 5, (1), pp. 21-39
- 30 Hannan, M.A., Abbas, S.M., Samad, S.A., and Hussain, A.: 'Modulation techniques for biomedical implanted devices and their challenges', *Sensors*, 2012, 12, (1), pp. 297-319
- 31 Gong, C.-S.A., Shiue, M.-T., Yao, K.-W., Chen, T.-Y., Chang, Y., and Su, C.-H.: 'A truly low-cost high-efficiency ASK demodulator based on self-sampling scheme for bioimplantable applications', *IEEE Transactions on Circuits and Systems I: Regular Papers*, 2008, 55, (6), pp. 1464-1477
- 32 Bensky, A.: 'Short-range Wireless Communication: Fundamentals of RF System Design and Application, Newnes', in Editor (Ed.)<sup>(Eds.)</sup>: 'Book Short-range Wireless Communication: Fundamentals of RF System Design and Application, Newnes' (Oxford, 2004, edn.), pp.
- 33 Kao, C.-H., and Tang, K.-T.: 'Wireless power and data transmission with ASK demodulator and power regulator for a biomedical implantable SOC', in Editor (Ed.)<sup>(Eds.)</sup>: 'Book Wireless power and data transmission with ASK demodulator and power regulator for a biomedical implantable SOC' (IEEE, 2009, edn.), pp. 179-182
- 34 Daoud, D., Ghorbel, M., Hamida, A.B., and Tomas, J.: 'Fully integrated CMOS data and clock recovery for wireless biomedical implants', in Editor (Ed.)<sup>(Eds.)</sup>: 'Book Fully integrated CMOS data and clock recovery for wireless biomedical implants' (IEEE, 2011, edn.), pp. 1-5
- 35 Gudnason, G.: 'A low-power ASK demodulator for inductively coupled implantable electronics', in Editor (Ed.)<sup>(Eds.)</sup>: 'Book A low-power ASK demodulator for inductively coupled implantable electronics' (IEEE, 2000, edn.), pp. 385-388
- 36 Zhu, K., Haider, M.R., Yuan, S., and Islam, S.K.: 'A sub-1 $\mu$ A low-power FSK modulator for biomedical sensor circuits', in Editor (Ed.)<sup>(Eds.)</sup>: 'Book A sub-1 $\mu$ A low-power FSK modulator for biomedical sensor circuits' (IEEE, 2010, edn.), pp. 265-268
- 37 Jung, L.H., Byrnes-Preston, P., Hessler, R., Lehmann, T., Suaning, G., and Lovell, N.H.: 'A dual band wireless power and FSK data telemetry for biomedical implants', in Editor (Ed.)<sup>(Eds.)</sup>: 'Book A dual band wireless power and FSK data telemetry for biomedical implants' (IEEE, 2007, edn.), pp. 6596-6599
- 38 Ghovanloo, M., and Najafi, K.: 'A wideband frequency-shift keying wireless link for inductively powered biomedical implants', *IEEE Transactions on Circuits and Systems I: Regular Papers*, 2004, 51, (12), pp. 2374-2383
- 39 Zgaren, M., and Sawan, M.: 'A low-power dual-injection-locked RF receiver with FSK-to-OOK conversion for biomedical implants', *IEEE Transactions on Circuits and Systems I: Regular Papers*, 2015, 62, (11), pp. 2748-2758
- 40 Abdelhalim, K., Kokarovtseva, L., Velazquez, J.L.P., and Genov, R.: '915-MHz FSK/OOK wireless neural recording SoC with 64 mixed-signal FIR filters', *IEEE Journal of Solid-State Circuits*, 2013, 48, (10), pp. 2478-2493
- 41 Moradi, A., Zgaren, M., and Sawan, M.: 'A 0.084 nJ/b FSK transmitter and 4.8  $\mu$ W OOK receiver for ISM-band medical sensor networks', in Editor (Ed.)<sup>(Eds.)</sup>: 'Book A 0.084 nJ/b FSK transmitter and 4.8  $\mu$ W OOK receiver for ISM-band medical sensor networks' (IEEE, 2013, edn.), pp. 1-4
- 42 Xu, W., Luo, Z., and Sonkusale, S.: 'Fully digital BPSK demodulator and multilevel LSK back telemetry for biomedical implant transceivers', *IEEE Transactions on Circuits and Systems II: Express Briefs*, 2009, 56, (9), pp. 714-718
- 43 Luo, Z., and Sonkusale, S.: 'A novel BPSK demodulator for biological implants', *IEEE Transactions on Circuits and Systems I: Regular Papers*, 2008, 55, (6), pp. 1478-1484
- 44 Kim, J., Chae, M.S., Wu, L., and Liu, W.: 'A fully integrated DPSK demodulator for high density biomedical implants', in Editor (Ed.)<sup>(Eds.)</sup>: 'Book A fully integrated DPSK demodulator for high density biomedical implants' (IEEE, 2008, edn.), pp. 93-96
- 45 Elamary, G., Chester, G., and Neasham, J.: 'A simple digital VHDL QPSK modulator designed using CPLD/FPGAs for biomedical devices applications', in Editor (Ed.)<sup>(Eds.)</sup>: 'Book A simple digital VHDL QPSK modulator designed using CPLD/FPGAs for biomedical devices applications' (2009, edn.), pp. 978-988
- 46 Hu, Y., and Sawan, M.: 'A fully integrated low-power BPSK demodulator for implantable medical devices', *IEEE Transactions on Circuits and Systems I: Regular Papers*, 2005, 52, (12), pp. 2552-2562
- 47 Simard, G., Sawan, M., and Massicotte, D.: 'High-speed OQPSK and efficient power transfer through inductive link for biomedical implants', *IEEE Transactions on biomedical circuits and systems*, 2010, 4, (3), pp. 192-200
- 48 Sokal, N.O., and Sokal, A.D.: 'Class EA new class of high-efficiency tuned single-ended switching power amplifiers', *IEEE Journal of solid-state circuits*, 1975, 10, (3), pp. 168-176

- 49 Green, P.B.: 'Class-E power amplifier design for wireless power transfer', Infineon, Appl. Note 1803, 2018, pp. 1-51
- 50 Navaii, M.L., Sadjedi, H., and Sarrafzadeh, A.: 'Efficient ASK data and power transmission by the class-E with a switchable tuned network', IEEE Transactions on Circuits and Systems I: Regular Papers, 2018, 65, (10), pp. 3255-3266
- 51 Lee, E.K.: 'A discrete controlled fully integrated class E coil driver with power efficient ASK modulation for powering biomedical implants', IEEE Transactions on Circuits and Systems I: Regular Papers, 2015, 62, (6), pp. 1678-1687
- 52 Teh, Y.-K., Mohd-Yasin, F., Choong, F., Reaz, M.I., and Kordesch, A.V.: 'Design and analysis of UHF micropower CMOS DTMOST rectifiers', IEEE Transactions on Circuits and Systems II: Express Briefs, 2009, 56, (2), pp. 122-126
- 53 Mutashar, S., Hannan, M., Samad, S.A., and Hussain, A.: 'Efficient data and power transfer for bio-implanted devices based on ASK modulation techniques', Journal of Mechanics in Medicine and Biology, 2012, 12, (05), pp. 1240030
- 54 Hmida, G.B., Dhieb, M., Ghariani, H., and Samet, M.: 'Transcutaneous power and high data rate transmission for biomedical implants', in Editor (Ed.)^(Eds.): 'Book Transcutaneous power and high data rate transmission for biomedical implants' (IEEE, 2006, edn.), pp. 374-378
- 55 Mutashar, S., and Hannan, M.A.: 'Efficient low-power recovery circuits for bio-implanted micro-sensors', Przegląd elektrotechniczny (ERJ), 2013, 89, (5), pp. 15-18
- 56 Wang, C.-C., Lee, T.-J., Chio, U.F., Hsiao, Y.-T., and Chen, J.-J.J.: 'A 570-kbps ASK demodulator without external capacitors for low-frequency wireless bio-implants', Microelectronics Journal, 2008, 39, (1), pp. 130-136

# Appendix

## 1. Measurements Data (Figures 41, 42, 43, 44, 46)

### a) Wireless power transfer without data modulation

| Wireless Power Transfer (Supply at 3V) |                  |                         |                 |                   |                |
|--|------------------|-------------------------|-----------------|-------------------|----------------|
| Distance (cm)                          | Load Voltage (V) | Transmitter Current (A) | DC Power In (W) | DC Power Out (mW) | PTE (Pout/Pin) |
| 0,9                                    | 4,93             | 0,247                   | 0,741           | 5,17              | 0,007          |
| 1,2                                    | 4,11             | 0,234                   | 0,702           | 3,59              | 0,005          |
| 1,5                                    | 3,13             | 0,198                   | 0,594           | 2,08              | 0,004          |
| 1,8                                    | 1,71             | 0,169                   | 0,507           | 0,62              | 0,001          |
| 2,1                                    | 0,97             | 0,159                   | 0,477           | 0,20              | 0,000          |
| 2,4                                    | 0,61             | 0,155                   | 0,465           | 0,08              | 0,000          |
| 2,7                                    | 0,32             | 0,151                   | 0,453           | 0,02              | 0,000          |
| 3,0                                    | 0,2              | 0,15                    | 0,45            | 0,01              | 0,000          |

| Wireless Power Transfer (Supply at 4V) |                  |                         |                 |                   |                |
|--|------------------|-------------------------|-----------------|-------------------|----------------|
| Distance (cm)                          | Load Voltage (V) | Transmitter Current (A) | DC Power In (W) | DC Power Out (mW) | PTE (Pout/Pin) |
| 0,9                                    | 6                | 0,368                   | 1,472           | 7,66              | 0,005          |
| 1,2                                    | 5,3              | 0,348                   | 1,392           | 5,98              | 0,004          |
| 1,5                                    | 4,02             | 0,285                   | 1,14            | 3,44              | 0,003          |
| 1,8                                    | 3,15             | 0,256                   | 1,024           | 2,11              | 0,002          |
| 2,1                                    | 2,05             | 0,237                   | 0,948           | 0,89              | 0,001          |
| 2,4                                    | 1,551            | 0,231                   | 0,924           | 0,51              | 0,001          |
| 2,7                                    | 0,77             | 0,224                   | 0,896           | 0,13              | 0,000          |
| 3,0                                    | 0,51             | 0,222                   | 0,888           | 0,06              | 0,000          |

| Wireless Power Transfer (Supply at 5V) |              |                     |             |              |     |
|--|--------------|---------------------|-------------|--------------|-----|
| Distance                               | Load Voltage | Transmitter Current | DC Power In | DC Power Out | PTE |

| (cm) | (V)   | (A)   | (W)   | (mW) | (Pout/Pin) |
|------|-------|-------|-------|------|------------|
| 0,9  | 6     | 0,456 | 2,28  | 7,66 | 0,003      |
| 1,2  | 5,79  | 0,438 | 2,19  | 7,13 | 0,003      |
| 1,5  | 4,75  | 0,391 | 1,955 | 4,80 | 0,002      |
| 1,8  | 3,72  | 0,346 | 1,73  | 2,94 | 0,002      |
| 2,1  | 3,06  | 0,238 | 1,19  | 1,99 | 0,002      |
| 2,4  | 1,99  | 0,313 | 1,565 | 0,84 | 0,001      |
| 2,7  | 1,18  | 0,306 | 1,53  | 0,30 | 0,000      |
| 3,0  | 0,854 | 0,303 | 1,515 | 0,16 | 0,000      |

| Wireless Power Transfer (Supply at 5.8V) |                  |                         |                 |                   |                |
|--|------------------|-------------------------|-----------------|-------------------|----------------|
| Distance (cm)                            | Load Voltage (V) | Transmitter Current (A) | DC Power In (W) | DC Power Out (mW) | PTE (Pout/Pin) |
| 0,9                                      | 6                | 0,5                     | 2,9             | 7,66              | 0,003          |
| 1,2                                      | 6                | 0,48                    | 2,784           | 7,66              | 0,003          |
| 1,5                                      | 4,67             | 0,426                   | 2,4708          | 4,64              | 0,002          |
| 1,8                                      | 3,57             | 0,43                    | 2,494           | 2,71              | 0,001          |
| 2,1                                      | 3,11             | 0,418                   | 2,4244          | 2,06              | 0,001          |
| 2,4                                      | 2,62             | 0,404                   | 2,3432          | 1,46              | 0,001          |
| 2,7                                      | 1,85             | 0,414                   | 2,4012          | 0,73              | 0,000          |
| 3,0                                      | 1,14             | 0,403                   | 2,3374          | 0,28              | 0,000          |

b) Wireless power transfer with data modulation at 100kHz

| Wireless Power Transfer (3V, 100kHz) |                  |                         |                 |                   |                |
|--------------------------------------|------------------|-------------------------|-----------------|-------------------|----------------|
| Distance (cm)                        | Load Voltage (V) | Transmitter Current (A) | DC Power In (W) | DC Power Out (mW) | PTE (Pout/Pin) |
| 0,9                                  | 4,1              | 0,169                   | 0,507           | 3,58              | 0,007          |
| 1,2                                  | 3,46             | 0,182                   | 0,546           | 2,55              | 0,005          |
| 1,5                                  | 2,45             | 0,171                   | 0,513           | 1,28              | 0,002          |

|     |       |       |       |      |       |
|-----|-------|-------|-------|------|-------|
| 1,8 | 1,36  | 0,14  | 0,42  | 0,39 | 0,001 |
| 2,1 | 1,125 | 0,126 | 0,378 | 0,27 | 0,001 |
| 2,4 | 0,736 | 0,121 | 0,363 | 0,12 | 0,000 |
| 2,7 | 0,416 | 0,117 | 0,351 | 0,04 | 0,000 |
| 3,0 | 0,178 | 0,113 | 0,339 | 0,01 | 0,000 |

| <b>Wireless Power Transfer (4V, 100kHz)</b> |                         |                                |                        |                          |                       |
|---|-------------------------|--------------------------------|------------------------|--------------------------|-----------------------|
| <b>Distance (cm)</b>                        | <b>Load Voltage (V)</b> | <b>Transmitter Current (A)</b> | <b>DC Power In (W)</b> | <b>DC Power Out (mW)</b> | <b>PTE (Pout/Pin)</b> |
| 0,9   | 5,4                     | 0,291                          | 1,164                  | 6,20                     | 0,005                 |
| 1,2   | 4,026                   | 0,257                          | 1,028                  | 3,45                     | 0,003                 |
| 1,5   | 3,16                    | 0,212                          | 0,848                  | 2,12                     | 0,003                 |
| 1,8   | 2,092                   | 0,189                          | 0,756                  | 0,93                     | 0,001                 |
| 2,1   | 1,47                    | 0,182                          | 0,728                  | 0,46                     | 0,001                 |
| 2,4   | 1,1                     | 0,177                          | 0,708                  | 0,26                     | 0,000                 |
| 2,7   | 0,7                     | 0,174                          | 0,696                  | 0,10                     | 0,000                 |
| 3,0   | 0,356                   | 0,171                          | 0,684                  | 0,03                     | 0,000                 |

| <b>Wireless Power Transfer (5V, 100kHz)</b> |                         |                                |                        |                          |                       |
|---|-------------------------|--------------------------------|------------------------|--------------------------|-----------------------|
| <b>Distance (cm)</b>                        | <b>Load Voltage (V)</b> | <b>Transmitter Current (A)</b> | <b>DC Power In (W)</b> | <b>DC Power Out (mW)</b> | <b>PTE (Pout/Pin)</b> |
| 0,9   | 6                       | 0,384                          | 1,92                   | 7,66                     | 0,004                 |
| 1,2   | 5,15                    | 0,365                          | 1,825                  | 5,64                     | 0,003                 |
| 1,5   | 4,47                    | 0,335                          | 1,675                  | 4,25                     | 0,003                 |
| 1,8   | 3,49                    | 0,299                          | 1,495                  | 2,59                     | 0,002                 |
| 2,1   | 3,3                     | 0,294                          | 1,47                   | 2,32                     | 0,002                 |
| 2,4   | 1,88                    | 0,272                          | 1,36                   | 0,75                     | 0,001                 |
| 2,7   | 1,19                    | 0,263                          | 1,315                  | 0,30                     | 0,000                 |
| 3,0   | 0,72                    | 0,26                           | 1,3                    | 0,11                     | 0,000                 |

| <b>Wireless Power Transfer (6V, 100kHz)</b> |                         |                                |                        |                          |                       |
|---|-------------------------|--------------------------------|------------------------|--------------------------|-----------------------|
| <b>Distance (cm)</b>                        | <b>Load Voltage (V)</b> | <b>Transmitter Current (A)</b> | <b>DC Power In (W)</b> | <b>DC Power Out (mW)</b> | <b>PTE (Pout/Pin)</b> |
| 0,9   | 6                       | 0,443                          | 2,658                  | 7,66                     | 0,003                 |
| 1,2   | 5,1                     | 0,406                          | 2,436                  | 5,53                     | 0,002                 |
| 1,5   | 4,29                    | 0,37                           | 2,22                   | 3,92                     | 0,002                 |
| 1,8   | 3,54                    | 0,341                          | 2,046                  | 2,67                     | 0,001                 |
| 2,1   | 2,915                   | 0,326                          | 1,956                  | 1,81                     | 0,001                 |
| 2,4   | 2,3                     | 0,316                          | 1,896                  | 1,13                     | 0,001                 |
| 2,7   | 1,574                   | 0,31                           | 1,86                   | 0,53                     | 0,000                 |
| 3,0   | 0,985                   | 0,305                          | 1,83                   | 0,21                     | 0,000                 |

c) Maximum detectable frequency

| <b>Maximum Detectable Frequency in kHz (MI at 50%)</b> |             |           |           |           |           |
|--|-------------|-----------|-----------|-----------|-----------|
| <b>Distance (cm)</b>                                   | <b>6.6V</b> | <b>6V</b> | <b>5V</b> | <b>4V</b> | <b>3V</b> |
| 0,9  |             | 20        | 60        | 155       | 90        |
| 1,2  | 200         | 190       | 140       | 105       | 100       |
| 1,5  | 165         | 165       | 130       | 110       | 75        |
| 1,8  | 165         | 140       | 115       | 85        | 115       |
| 2,1  | 135         | 115       | 90        | 95        | 80        |
| 2,4  | 100         | 100       | 115       | 55        |           |
| 2,7  | 110         | 115       | 65        |           |           |
| 3,0  | 120         | 80        |           |           |           |

2. LTSPICE netlist

\* C:\Users\vassil\Documents\LTspiceXVII\modulator\_10c.asc

Q1 N010 BE2 IN 0 2SCR293P

Q2 N010 BE1 BE2 0 2SCR293P

V1 N010 0 10

R1 N010 BE1 3k

R2 BE1 N011 6k  
M1 N011 data 0 0 RUC002N05  
V2 data 0 PULSE(0 5 0 30f 30f 0.000001666 0.000003333)  
L1 IN N014 3.3  
C1 N018 N014 110p  
C2 0 N014 90p  
L2 N018 N019 1.4  
L3 N019 N022 1.54781 Rser=1.3199  
C3 OUT N022 100p  
V3 N017 0 PULSE(0 5 0 30f 30f 0.000000036873156 0.00000007374631)  
L4 transm 0 1.54781 Rser=1.3199  
C4 N020 transm 470p  
C5 0 N021 470p  
C6 0 N016 470p  
C7 0 N013 470p  
C8 transm N015 470p  
C9 transm N012 470p  
D1 0 N020 MBR0520L  
D2 N020 N021 MBR0520L  
D3 N021 N015 MBR0520L  
D4 N015 N016 MBR0520L  
D5 N016 N012 MBR0520L  
D6 N012 N013 MBR0520L  
C10 transm 0 94.35p  
R3 N013 0 5k  
C11 IN 0 1p  
XU1 N014 N017 0 irlml2030  
M2 transm N023 0 0 RUC002N05  
V5 N023 0 PULSE(0 0 0 30f 30f 0.000005 0.00002)  
V6 N002 0 5  
C15 N006 0 1p  
R6 N003 N005 600k  
C16 0 N003 1n  
C17 0 N005 100p  
D8 N004 N005 RB751G-40

```
R7 0 N005 160k
XU2 N003 N005 N002 0 N006 TS881
V4 N007 0 5
C12 comp_out 0 1p
R4 N008 N009 100k
C13 0 N008 100p
C14 0 N009 10p
D7 transm N009 RB751G-40
R5 0 N009 50k
XU3 N008 N009 N007 0 comp_out TS881
D9 0 N013 BZX84B6V2L
C19 OUT 0 1.5n
M3 N001 OUT N004 N004 RUC002N05
V7 N001 0 5
R8 N004 0 5k
R9 OUT 0 100k
C18 N013 0 C
.model D D
.lib C:\Users\vassi\Documents\LTspiceXVII\lib\cmp\standard.dio
.model NPN NPN
.model PNP PNP
.lib C:\Users\vassi\Documents\LTspiceXVII\lib\cmp\standard.bjt
.model NMOS NMOS
.model PMOS PMOS
.lib C:\Users\vassi\Documents\LTspiceXVII\lib\cmp\standard.mos
.tran 0 40m 0
K L3 L4 0.4
.ic V(n003)=4.65 V(n005)=4.66
.lib C:\Users\vassi\Desktop\TS881_macromodel_PSPICE (New Pins Order).mod
.lib C:\Users\vassi\Downloads\lrlml2030.spi
.backanno
.end
```